
Studies on Linear and Fast Drift Gases for ATLAS MDT Chambers

Nicola Tyler



Munich 2011

Studies on Linear and Fast Drift Gases for ATLAS MDT Chambers

Nicola Tyler

Master Thesis
at the Faculty of Physics
Ludwig-Maximilians-Universität
München

by
Nicola Tyler
born in Munich

Munich, 26th August 2011

Advisor: Prof. Dr. Otmar Biebel

Contents

Summary	xiii
1 Introduction	1
1.1 Large Hadron Collider	1
1.2 ATLAS Detector	2
1.3 Selection of the Current Drift Gas Ar:CO ₂ 93:7	2
1.4 Motivation for Drift Gas Studies	3
2 MDT Chambers	5
2.1 Design and Working Principle	5
2.2 Theory of Drift Tubes	8
2.2.1 Interaction of Charged Particles with Gaseous Matter	8
2.2.2 Drift and Diffusion of Ions and Electrons	9
2.2.3 Electrons in Large Electric Fields	12
2.2.4 Cylindrical Counters	12
2.3 Problems with Ar:CO ₂ 93:7	14
2.4 Requirements for Drift Gases	15
3 Simulations	17
3.1 Drift Velocity	18
3.2 Linearity	21
3.3 Maximum Drift Time	23
3.4 Influence of the Anode Voltage	26
3.5 Summary	27
4 Experimental Results for Ar:CO₂ and Ar:CO₂:N₂ Gas Mixtures	29
4.1 Experimental Set-Up	29
4.2 Data Acquisition	30
4.3 Data Analysis	32
4.3.1 Drift Time Spectrum	32
4.3.2 RT-Relation	34
4.3.3 Signal Height	36
4.3.4 End of Signal	37

4.3.5	Streamer	37
4.4	Results for Ar:CO ₂ Gas Mixtures	37
4.5	Operation at Different Voltages	40
4.5.1	Drift Time Spectrum and RT-Relation	40
4.5.2	Signal Height and End of Signal	40
4.6	Results for Ar:CO ₂ :N ₂ Gas Mixtures at Gas Gain 20 000	42
4.7	Afterpulsing	44
4.7.1	Averaged FADC Signals	44
4.7.2	FADC Pulses after Maximum Drift Time	45
4.7.3	Physical Approach	50
4.7.4	Afterpulse Amplitudes and Integrated Afterpulse Spectra	52
4.7.5	Streamer Signals	53
4.7.6	Single Events	54
4.8	Summarized Experimental Results	55
4.8.1	Maximum Drift Time	58
4.8.2	Linearity	60
4.8.3	Voltage for Gas Gain 20 000	61
4.8.4	Afterpulsing	61
4.8.5	Afterpulse Amplitude Spectra and Integrated Afterpulse Spectra	62
4.8.6	Time after which Signals have Dropped Down	63
4.8.7	Streamer Properties	63
4.8.8	Summary	64
5	Conclusions	65
	Acknowledgment	69

List of Figures

1.1	LHC Schematic View	2
1.2	ATLAS Detector	3
2.1	ATLAS MDT Chamber	6
2.2	Muon Track Reconstruction in MDT Chamber	7
2.3	Cross Section through Single Drift Tube	7
2.4	Electric Field inside Drift Tube	8
2.5	Electron Cross Sections in Argon	10
2.6	Mean Energy Loss Rate of Gaseous Helium	10
2.7	Electron Cross Sections in Carbon Dioxide	11
2.8	Electron Cross Sections in Nitrogen	11
2.9	Diffusion vs Drift	11
2.10	Operation Modes of Cylindrical Counters	13
2.11	Spatial Resolution of ATLAS Muon Chambers under Irradiation	14
2.12	Simulated Drift Velocity	14
3.1	Simulated Ar:CO ₂ Drift Velocities against Electric Field, 0% N ₂	18
3.2	Simulated Ar:CO ₂ Drift Velocities against Drift Radius, 0% N ₂	18
3.3	Simulated Drift Velocities against Electric Field with Fixed Ratio Ar:CO ₂ 96:4 and Addition of N ₂ up to 3%	19
3.4	Simulated Drift Velocities against Drift Radius with Fixed Ratio Ar:CO ₂ 96:4 and Addition of N ₂ up to 3%	19
3.5	Simulated Drift Velocities against Electric Field with 1% N ₂ and Variation of Ar:CO ₂	20
3.6	Simulated Drift Velocities against Drift Radius with 1% N ₂ and Variation of Ar:CO ₂	20
3.7	Measure for Linearity	21
3.8	Simulated Linearities for CO ₂ between 1% and 10% and N ₂ between 0% and 10%	21
3.9	Simulated Linearities for fixed Ar:CO ₂ ratios under N ₂ Addition up to 3%; CO ₂ up to 10%	22
3.10	Simulated Linearities for fixed Ar:CO ₂ ratios under N ₂ addition up to 3%; CO ₂ up to 4%	22

3.11 Simulated Maximum Drift Times for CO ₂ between 1% and 10% and N ₂ between 0% and 10%	23
3.12 Simulated Maximum Drift Times for Different Fixed Ar:CO ₂ Ratios; Addition of N ₂ of up to 3%; CO ₂ Contents between 1% and 10%	24
3.13 Simulated Maximum Drift Times for Different Fixed Ar:CO ₂ Ratios; Addition of N ₂ of up to 3%. CO ₂ Contents between 1% and 6%	25
3.14 Influence of Voltage on Drift Velocity, Ar:CO ₂ 94:6	26
3.15 Influence of Voltage on Drift Velocity, Ar:CO ₂ 96:4	26
3.16 Influence of Voltage on Drift Velocity, Ar:CO ₂ :N ₂ 96:3.5:0.5	26
3.17 Influence of Voltage on Drift Velocity, Ar:CO ₂ :N ₂ 96:3:1	26
4.1 Experimental Set-Up	29
4.2 Readout and Trigger Logic	29
4.3 Characteristic FADC Signal	31
4.4 Geometrical Considerations on Signal Generation	31
4.5 Signal Shape Explanation	31
4.6 Analysis of Flash-ADC Signal	32
4.7 TDC Drift Time Spectrum Ar:CO ₂ 93:7	33
4.8 Ideal Drift Time Spectrum	33
4.9 Determination of t_{min} and t_{max}	34
4.10 Ideal Drift Velocity	35
4.11 RT-Relation Ar:CO ₂ 93:7	35
4.12 Ideal RT-Relation	35
4.13 Signal Height Spectrum Ar:CO ₂ 93:7	36
4.14 End of Signal Spectrum Ar:CO ₂ 93:7	36
4.15 Experiment: Ar:CO ₂ Drift Time Spectra 3080 V	38
4.16 Experiment: Ar:CO ₂ RT-Relations 3080 V	38
4.17 Experiment: Ar:CO ₂ Drift Time Spectra Gas Gain 20 000	38
4.18 Experiment: Ar:CO ₂ RT-Relations Gas Gain 20 000	38
4.19 Experiment: Ar:CO ₂ Signal Height Spectra 3080 V	39
4.20 Experiment: Ar:CO ₂ End of Signal Spectra 3080 V	39
4.21 Experiment: Ar:CO ₂ Signal Height Spectra Gas Amplification 20 000	39
4.22 Experiment: Ar:CO ₂ End of Signal Spectra Gas Amplification 20 000	39
4.23 Experiment: Ar:CO ₂ 96:4 Drift Time Spectra, 3080 V and 2970 V	40
4.24 Experiment: Ar:CO ₂ 96:4 RT-Relation, 3080 V and 2970 V	40
4.25 Experiment: Ar:CO ₂ 96:4 Signal Height Spectra, 3080 V and 2970 V	41
4.26 Experiment: Ar:CO ₂ 96:4 Signal Height FADC Signals, 3080 V and 2970 V	41
4.27 Experiment: Ar:CO ₂ 96:4 End of Signal Spectra, 3080 V and 2970 V	42
4.28 Experiment: Ar:CO ₂ :N ₂ Drift Time Spectra	43
4.29 Experiment: Ar:CO ₂ :N ₂ RT-Relations	43
4.30 Experiment: Ar:CO ₂ :N ₂ Signal Height Spectra	44
4.31 Experiment: Ar:CO ₂ :N ₂ End of Signal Spectra	44
4.32 Averaged Signals Ar:CO ₂ 93:7, 3080 V	45

4.33	Averaged Signals for Ar:CO ₂ 96:4, 2970 V	46
4.34	Averaged Signals for Ar:CO ₂ 97:3, 3080 V	46
4.35	Averaged Signals for Ar:CO ₂ :N ₂ 96:2:2, 3141 V	47
4.36	Averaged Signals for Ar:CO ₂ :N ₂ 97:2:1, 3080 V	47
4.37	Afterpulse - Misdetermination of End of Signal	47
4.38	End of Signal, Ar:CO ₂ :N ₂ 97:2:1, 3080V	47
4.39	Time Differences between First Pulses and Afterpulses	48
4.40	Scheme of Integrals in Terms of Maximum Drift Times	48
4.41	Integrals for Ar:CO ₂ 96:4 Averaged Signals in Intervals of t_{max}	49
4.42	Ratios of Integrals in Intervals of t_{max} for Ar:CO ₂ 96:4 Averaged Signals	49
4.43	Scheme of Physical Approach to Afterpulsing - Photo Effect at Tube Wall	51
4.44	Amplitude Spectra	52
4.45	Amplitude Spectra, Zoom	52
4.46	Integrated Afterpulse Spectra	53
4.47	Integrated Afterpulse Spectra	53
4.48	Integrated Afterpulse Spectra, Promising Gas Mixtures	54
4.49	Single Event Ar:CO ₂ 93:7, $t_{drift} = 111$ ns	55
4.50	Single Event Ar:CO ₂ 93:7, $t_{drift} = 420$ ns	55
4.51	Single event Ar:CO ₂ :N ₂ 97:2:1, 3080V $t_{drift} = 199$ ns	55
4.52	Single event Ar:CO ₂ :N ₂ 97:2:1, 3080V $t_{drift} = 342$ ns	55
4.53	Single Event Ar:CO ₂ :N ₂ 96:3:1, 3035V, $t_{drift} = 170$ ns	56
4.54	Single Event Ar:CO ₂ :N ₂ 96:3:1, 3035V, $t_{drift} = 320$ ns	56
4.55	Summary: Maximum Drift Time	58
4.56	Summary: Linearity	59
4.57	Summary: Voltage for Gas Gain 20 000	60
4.58	Summary: Afterpulsing	60
4.59	Summary: Afterpulse Amplitudes	62
4.60	Summary: Afterpulse Integrals	62
4.61	Summary: Time after which 70% of Signals are Quiet	63
4.62	Summary: Time after which 95% of Signals are Quiet	63
4.63	Summary: Number of large Signals	64

List of Tables

2.1	Features of Monitored Drift Tubes	6
3.1	Parameters Used for Simulations	18
3.2	N ₂ Minima of t_{max} for Constant Ar:CO ₂ Ratios	24
4.1	Summarized Experimental Results of Gas Mixtures at 3080 V	56
4.2	Summarized Experimental Results of Gas Mixtures at Gas Gain 20 000 . .	57

Summary

The ATLAS detector is a general purpose detector at the Large Hadron Collider (LHC) at the European Organization for Nuclear Research CERN. Part of the muon spectrometer of the ATLAS detector are the **M**onitored-**D**rift-**T**ube (MDT) detectors. They consist of several hundred drift tubes packed into multilayers and are aligned with the help of an optical monitoring system.

The drift tubes are filled with a gas mixture composed of argon and carbon dioxide in mixing ratio 93% to 7% per volume (Ar:CO₂ 93:7). Under high rates of background irradiation, as neutrons or gammas, this standard drift gas shows considerable deterioration in resolution and due to its relatively long maximum drift time close to 1 μ s high occupancy. Due to the LHC luminosity upgrade from currently $3 \cdot 10^{33} \text{ cm}^{-2}\text{s}^{-1}$ to $5 \cdot 10^{34} \text{ cm}^{-2}\text{s}^{-1}$, we try to reduce the sensitivity of the MDT chambers on background irradiation. The main reason for the resolution deterioration of Ar:CO₂ 93:7 is the non-linearity of the rt -relation, meaning that the electron drift velocity depends strongly on the electric field.

This thesis contributes to the search for an alternative drift gas for the ATLAS MDT chambers. The focus lies on inert, linear and considerably faster drift gases containing argon, carbon dioxide and nitrogen.

Various Ar:CO₂:N₂ gas mixtures were systematically simulated. The most linear gas mixtures contain between 1% and 3% CO₂. For 1% and 2% CO₂, the addition of small N₂ amounts up to 1.5% is preferable. The fastest mixtures contain between 2% and 4% CO₂. Small amounts of N₂ up to 1.2% show a positive effect on the maximum drift time. The studied reduction of the anode voltage from 3080 V to 2970 V did not show significant changes in the drift velocity.

Furthermore, Ar:CO₂ and Ar:CO₂:N₂ gas mixtures were investigated experimentally. The measurements are analyzed with respect to linearity, maximum drift time, afterpulsing and streamer probability. The fastest gas mixture, Ar:CO₂:N₂ 97:2.5:0.5, is 38% faster than the standard mixture. Similar to the simulations, fast mixtures contain between 2% and 4% CO₂ and linear gas mixtures contain between 1% and 4% CO₂. The addition of small amounts of N₂ (from 0.5% to 1%) shows improvement in maximum drift time for gas mixtures in the low CO₂ range and small deterioration in linearity within the studied

N_2 range of 0.5% to 3%. Afterpulsing has been observed. However, the signals of fast gas mixtures with afterpulsing end still earlier than slow mixtures without afterpulsing.

The candidate Ar:CO₂:N₂ 96:3:1 was tested on ageing effects at the tandem accelerator in Garching [24]. Drift tubes filled with this mixture were irradiated with 100 nA of 20 MeV protons. The irradiation spot was $70 \cdot 5 \text{ mm}^2$. Within half a day of irradiation a charge of 1 C/cm was accumulated on the anode wire corresponding to about one lifetime of MDT tubes at ATLAS. No feature of ageing was observed during the subsequent cosmic muon measurement of the irradiated areas in comparison to non-irradiated areas.

The single tube resolution under use of Ar:CO₂:N₂ 96:3:1 was studied at the gamma-irradiation-facility (GIF) at CERN and at the cosmic-ray-measurement-facility in Garching [16]. The gas mixture 96:3:1 showed similar resolution as 93:7 without background irradiation, at gamma fluxes of up to 1900 Hz/cm^2 the spatial resolution deteriorated only marginal.

Accordingly, good candidates for an alternative drift gas are Ar:CO₂:N₂ 97:2.5:0.5, 96:3.5:0.5, 96:3:1 and Ar:CO₂ 97:3. The experimental and the simulated results of these gas mixtures are in good agreement. The results of 96:3:1, good spatial resolution, minor dependence on space charge effects under background irradiation, no ageing and substantial reduction of occupancy should hold for all of them.

Chapter 1

Introduction

1.1 Large Hadron Collider

To discover new elementary particles like the Higgs boson or constituents of super symmetry, and to understand the laws of nature, particle colliders with high collision energies are desirable. The LHC, the most powerful of all existing colliders, is estimated to reach center of mass energies of 14 TeV in a couple of years.

The LHC is contained in a circular tunnel of 27 km circumference and is located approximately 100 m meters below surface at the European Organization for Nuclear Research CERN, crossing the borders of France and Switzerland. Into the LHC protons are injected from the Super Proton Synchrotron (SPS) with an energy of 0.45 TeV. A schematic view is shown in figure 1.1.

There are six experiments located at LHC [3]:

- ATLAS (**A** **T**oroidal **L**HC **A**pparatu**S**)
- CMS (**C**ompact **M**uon **S**olenoid)
- ALICE (**A** **L**arge **I**on **C**ollider **E**xperiment)
- TOTEM (**T**OTal **E**lastic and diffractive cross section **M**easurement)
- LHCb (**L**arge **H**adron **C**ollider **b**eauty)
- LHCf (**L**arge **H**adron **C**ollider **f**orward)

Two of them, ATLAS and CMS, are all purpose detectors. This thesis is in the framework of the muon spectrometer of the ATLAS detector.

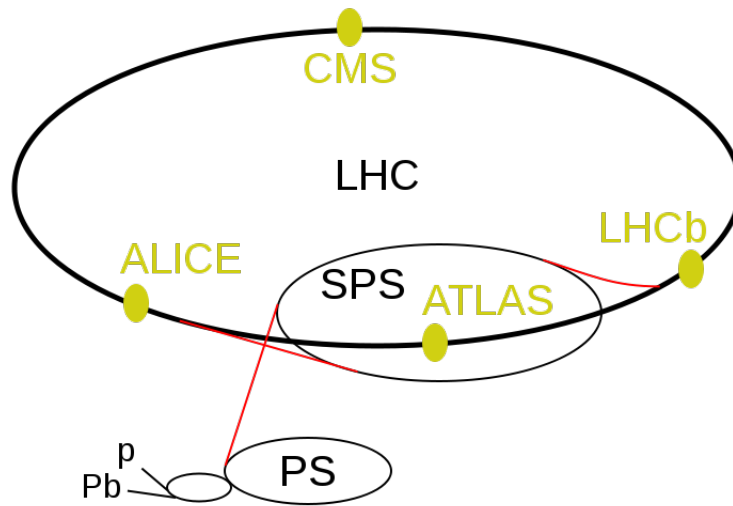


Figure 1.1: Schematic view of accelerators at CERN including the location of the four large LHC experiments ATLAS, CMS, ALICE and LHCb. [1]

1.2 ATLAS Detector

When a particle collision takes place inside the ATLAS detector, the tracks of the generated hadrons and charged leptons leave a message in the ATLAS detector. The detector is able to reconstruct their paths. Due to the magnetic field in the detector, charged particles are deflected, the radius of this curve is given by the momentum of the particle to be reconstructed.

Figure 1.2 shows an overview of the ATLAS detector. Each subsystem on the detector plays a different role in the reconstruction of particle energy or path. The path of muons is reconstructed with help of the muon spectrometer, the blue parts in figure 1.2. One of the subsystems of the spectrometer are the **Monitored-Drift-Tube** (MDT) chambers. Through-going muons leave a message in the tubes by ionizing the Ar:CO₂ gas inside the tubes.

1.3 Selection of the Current Drift Gas Ar:CO₂ 93:7

During the planning period of ATLAS, one of the first candidates for a drift gas for the MDT chambers was Ar:N₂:CH₄ 91:4:5 (argon, carbon dioxide and methane in mixing ratio 91% to 4% to 5%). This gas mixture is fast and linear and showed good resolution under irradiation [23]. However, tests on this gas mixture showed ageing effects [7]. Therefore, a new gas mixture without organic components was searched for. The newly selected gas mixture was Ar:CO₂ 93:7, which is currently used for the MDT chambers. The studies

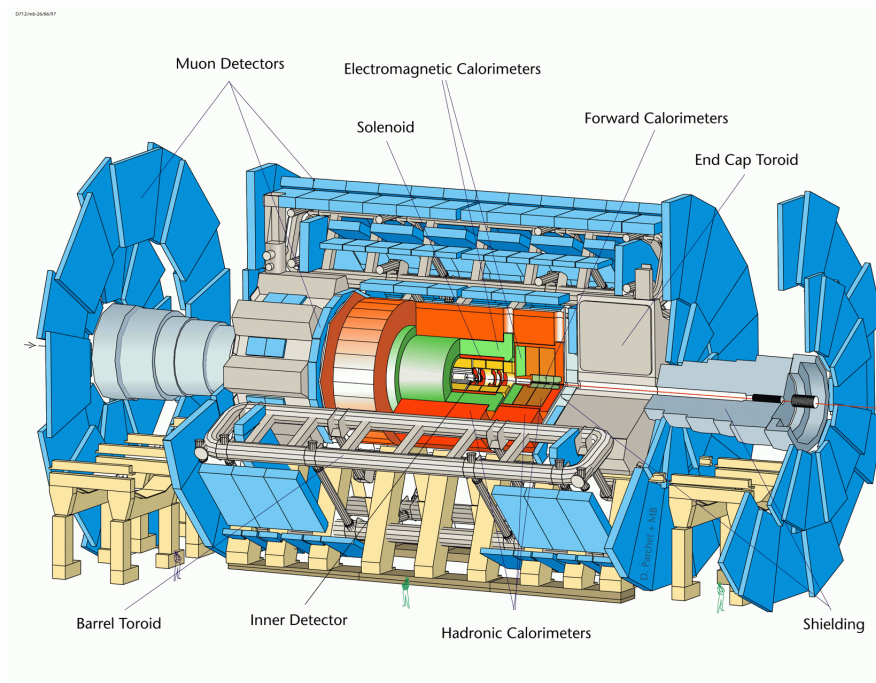


Figure 1.2: ATLAS detector. In blue: Muon spectrometer. It consists of the barrel and the endcap region. Each of them is subdivided in 3 layers of MDT chambers (inner, middle and outer layer). [2]

that lead to the election of this drift gas are described in [7] and [12].

The main difference in drift properties of $\text{Ar:N}_2:\text{CH}_4$ 91:4:5 and Ar:CO_2 93:7 is that $\text{Ar:N}_2:\text{CH}_4$ 91:4:5 is fast and linear, whereas Ar:CO_2 93:7 is slower and non-linear. Ar:CO_2 93:7 was selected as new drift gas, since it showed no ageing effects, good resolution and a small streamer rate of $< 0.1\%$ for gas gains of up to $4 \cdot 10^4$. Due to the non-linear rt -relation, the resolution under irradiation of Ar:CO_2 93:7 deteriorates a lot more than for the gas mixture $\text{Ar:N}_2:\text{CH}_4$ 91:4:5 with a linear rt -relation (further detail on this is described in section 2.3). However, without irradiation Ar:CO_2 93:7 shows a better resolution of $56 \mu\text{m}$, than $\text{Ar:N}_2:\text{CH}_4$ 91:4:5 with $79 \mu\text{m}$. Under gamma irradiation of 1400 Hz/cm^2 , the resolution deteriorates to $82 \mu\text{m}$ for Ar:CO_2 93:7 and $87 \mu\text{m}$ $\text{Ar:CO}_2:\text{CH}_4$, thus the new gas still shows better resolution (all numbers are extracted from [7]).

1.4 Motivation for Drift Gas Studies

Due to the luminosity upgrade at LHC from currently $3 \cdot 10^{33} \text{ cm}^{-2}\text{s}^{-1}$ to $5 \cdot 10^{34} \text{ cm}^{-2}\text{s}^{-1}$, the background rate will increase similarly and the sensibility to background events of the muon spectrometer has to be reduced. Replacement of the hardware is one solution. One

candidate as new hardware are drift tubes with halved diameter [11]. A more cost efficient solution is to find an alternative drift gas, which shows less resolution deterioration under irradiation. This thesis contributes to this search, and linear, fast and inorganic drift gases containing Ar:CO₂:N₂ are presented.

Chapter 2

MDT Chambers

This chapter explains the design, working principle and theoretical background of the Monitored-Drift-Tube chambers at the ATLAS muon spectrometer. As motivation for drift gas studies, the occurring problems under irradiation are presented and the requirements for an optimized drift gas are given.

2.1 Design and Working Principle

The MDT chambers aim to reconstruct the tracks of muons in order to determine their momenta. The following explains how the momentum can be gained from the reconstructed particle path. Due to the toroidal magnetic field in the barrel region of the ATLAS detector, charged particles follow a circular path. The curvature radius of this path is related to the momentum of the particle via

$$p = 0.3 \cdot r \cdot z \cdot B \quad (2.1)$$

where p [MeV] stands for particle momentum, r [m] for the curvature radius, z [1] for the charge of the particle and B [T] for the magnetic field strength. Since z and B are known, the particle momentum can be determined if the curvature radius is gained from the reconstructed particle track.

The local muon track is reconstructed by a single muon chamber. Figure 2.2 shows a cross section of two multilayers of six layers of drift tubes. For each drift tube that was traversed by a muon, the radius which indicates the shortest distance between the track and the center of the tube, is determined. This radius will be referred to as drift radius in the following. The local muon track can be reconstructed for the measured drift radii as shown in red in figure 2.2. The complete muon track inclusive the curvature is obtained by the combination of the three local muon tracks in the 3 layers of MDT chambers in the ATLAS muon spectrometer, see figure 1.2. The following will explain how the drift radii are obtained.

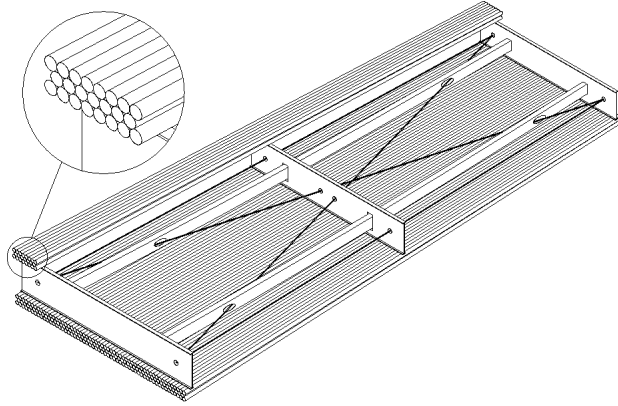


Figure 2.1: ATLAS Monitored Drift Tube chamber [6]

tube material	aluminum
wall thickness	0.4 mm
tube diameter	3 cm
tube length	3 m - 5 m
centrally tensioned	gold plated W-Re 97:3 wire, 350g
wire diameter	50 μm
voltage at wire	3080 V
electric field inside tube	proportional to $\frac{1}{r}$
filled with gas mixture	Ar:CO ₂ 93:7
pressure	3 bar absolute
gas gain	20 000

Table 2.1: Features of MDTs

Figure 2.1 shows a chamber with optical monitoring system to correct the chamber alignment for thermal movements or mechanical stress. A chamber consists of two multilayers, where each multilayer consists of three or four layers of drift tubes of up to 5 m length. The cross section of a single drift tube is shown in figure 2.3. The main features of the tubes are given in table 2.1.

The tubes consisting of aluminum with wall thickness 0.4 mm have an outer tube radius of 3 cm. Centrally, a gold plated 50 μm diameter tungsten-rhenium wire is tensioned along the tube length, which is on high voltage of 3080 V and creates an electric field inside the tube. The tungsten wire is positively charged with respect to the grounded cylinder resulting in an electric field proportional to r^{-1} as described in equation 2.2:

$$E(r) = \frac{+V}{\ln \frac{R_{\text{tube}}}{R_{\text{wire}}}} \cdot \frac{1}{r} \quad (2.2)$$

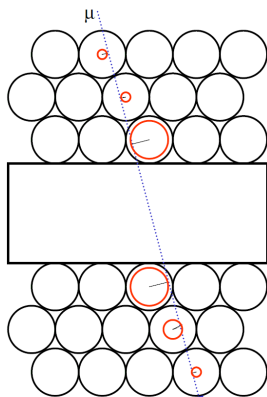


Figure 2.2: Cross section of two drift tube multi layers consisting of three layers each. Muon track reconstruction by fit to six drift radii (red circles). [28]

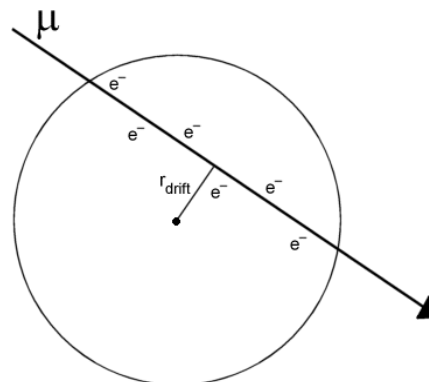


Figure 2.3: Cross section of a single drift tube. [28]

with the radial distance from the center r , anode voltage 3080 V and tube- and wire-radius R_{tube} and R_{wire} . The field ranges from 331.2 V/cm at the tube wall to 193 409.6 V/cm close the wire. The electric field against the tube radius is shown in figure 2.4. The tube is filled with a gas mixture of argon and carbon dioxide in mixing ratio 93 % to 7% per volume. This gas mixture will be referred to as Ar:CO₂ 93:7 in the following. The tubes are operated at a pressure of 3 bar absolute.

When a muon passes a tube, the gas inside the tube gets ionized and pairs of electrons and ions are created. Due to the electric field, the electrons drift towards the wire gaining kinetic energy. In a small region around the wire, the electrons have gained enough energy to ionize further gas atoms or molecules. These newly created electrons can lead to a further ionization processes and so on. This process is called gas amplification or gas gain and is described in detail in section 2.2.3. The amplification factor depends on the applied voltage and the gas mixture. The drift tubes operate in proportional modus resulting in numbers of electrons arriving at the wire that are proportional to the number of the primarily created electrons due to the muon passage.

In order to obtain the drift radius, the *drift time* is measured. The drift time refers to the time that electrons, created during the primary ionization process closest to the wire, need to drift towards the wire. This time can be gained when measuring the time that passes between the muon passage, which is given by the Resistive Plate Chambers in the barrel region and the Thin Gap Chambers in the forward region of the ATLAS detector [23] and the arrival of the first electrons at the anode wire. The electron drift velocity depends mainly on the gas mixture. For a given gas mixture the **radius-time-relation** relates drift times to drift radii. How this rt-relation is established is explained in section 4.3.2.

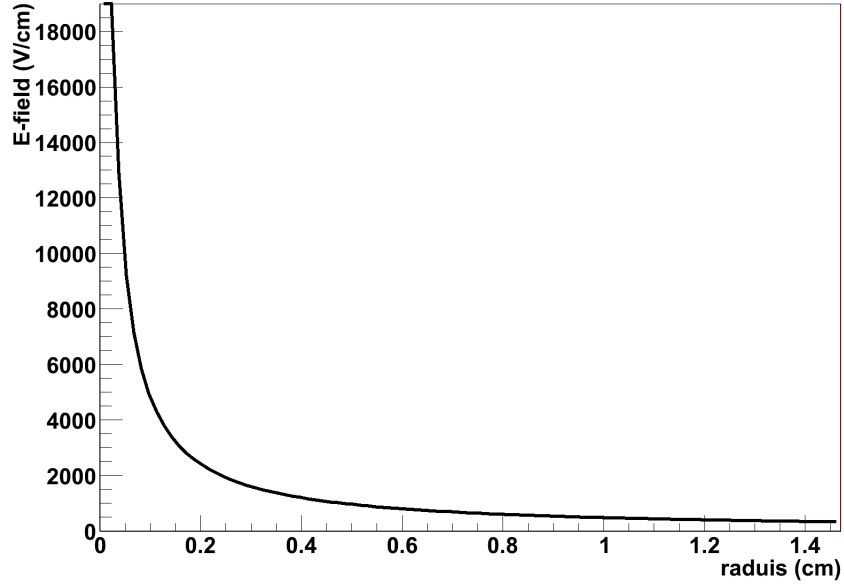


Figure 2.4: The electric field inside the drift tube is proportional to r^{-1} and is plotted against the tube radius. The maximum electric field is 193409 V/cm and the minimum electric field is 331.2 V/cm.

2.2 Theory of Drift Tubes

As explained in 2.1, the MDT chambers are filled with a gas mixture consisting of argon and carbon dioxide. Within the tubes exists an electric field. This section treats the physics of charged particles interacting with gaseous matter and the behaviour of electrons in gaseous matter and electric fields. Furthermore, the concept of proportional counters is explained. This section is based on [25], [21], [17] and [19].

2.2.1 Interaction of Charged Particles with Gaseous Matter

In case of the MDT chambers, a fast, charged particle - a muon - passes through gaseous matter. A charged particle interacts with gaseous matter most probably by electromagnetic interaction. Electromagnetic processes are ionization, bremsstrahlung, Cherenkov- and transition radiation.

The energy loss per unit length due to Coulomb interactions is described by the Bethe and Bloch formula [10]:

$$-\left\langle \frac{dE}{dX} \right\rangle = K z^2 \frac{Z}{A} \frac{1}{\beta^2} \left[\frac{1}{2} \ln \frac{2m_e c^2 \beta^2 \gamma^2 T_{max}}{I^2} - \beta^2 - \frac{\delta(\beta\gamma)}{2} \right] \quad (2.3)$$

where

$$K = \frac{4\pi N_A r_e^2 m_e^2 c^2}{A} \quad (2.4)$$

with the Avogadro number N_A , the electron mass and charge m_e and e , the atomic number of absorber Z , the atomic mass of absorber A , the ionization potential I . Charge and velocity of the projectiles are represented by z and β , respectively. T_{max} refers to the maximum kinetic energy that can be imparted to a free electron in a single collision. To this formula corrections have to be added, as shell corrections, for slow incident particles, and density corrections, concerning particles that are shielded from the full electric intensity due to the polarization of atoms along the particle path caused by the electric field of the incident particle. Furthermore the given formula for calculating the energy loss has to be modified, if the medium is not pure but a compound as weighted sum over the individual components [21].

The mean energy loss rate in gaseous helium and carbon, amongst others, is shown in figure 2.6. Since the energy loss scales with the atomic number of the absorber divided by the atomic mass, which is 0.5 for helium, 0.45 for argon and 1.2 for carbon, the energy loss curve for argon lies between the curve for helium and carbon.

2.2.2 Drift and Diffusion of Ions and Electrons

Ions and electrons in gaseous matter move without an electric field due to **diffusion**. If an electric field is applied, they move by **drifting** into the direction of the electric field in the case of positive ions, and in the opposite direction in case of electrons.

Ions

Diffusion is a movement without direction and takes place even in the absence of an electric field, originating from multiple collisions. Diffusion follows a Gaussian law [25] and can be described as in equation 2.5:

$$\frac{dN}{N} = \frac{1}{\sqrt{4\pi Dt}} e^{-(x^2/4Dt)} dx \quad (2.5)$$

where dN/N is the fraction of charges found in element dx at distance x from the origin after time t . The diffusion coefficient D depends on the gas mixture.

In case of an electric field a net movement of the ions is observed with an average drift velocity $v_{drift,ion}$ proportional to the electric field:

$$v_{drift,ion} = \mu^+ E \quad (2.6)$$

where μ^+ denotes the mobility of the ions, which independent of the electric field in the case of sufficiently large electric fields, since the average ion energy stays constant. In argon and carbon dioxide at 3 bar, the ion mobility is 0.52 cm²/Vs [16].

Electrons

The average energy of electrons changes with the electric field. The electron diffusion can be described by the same equation as for the ions, equation 2.5. However, in this case the diffusion coefficient depends on the electric field.

The drift velocity of electrons in electric fields follows from equation 2.7.

$$v_{drift,e} = \frac{e}{2m} E \tau \quad (2.7)$$

with the mean time between collisions τ depending on the electric field. This is due to the collision cross section variation with the electric field. For electrons moving slowly in a noble gas, the curve for the elastic cross sections shows a Ramsauer minimum and maximum [25]. This can be seen in figure 2.5 which displays the different cross sections for electrons in pure argon as function of their energy. More cross sections for electrons in carbon dioxide and nitrogen are shown in figures 2.7 and 2.8.

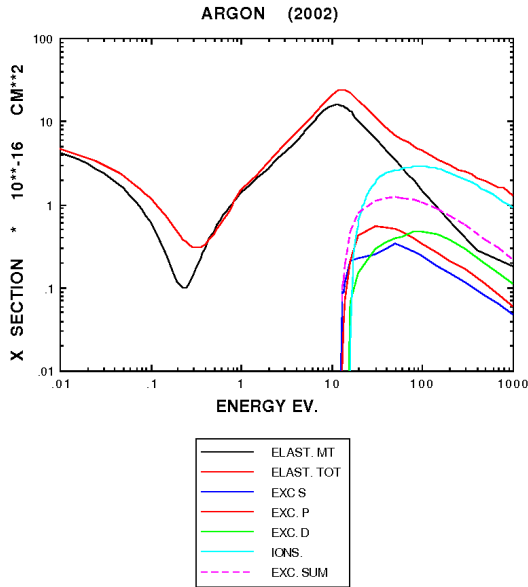


Figure 2.5: Cross sections of electrons in argon. For electrons moving slowly in a noble gas the cross section shows a minimum and a maximum when varying their energy. This effect is called Ramsauer effect. [5]

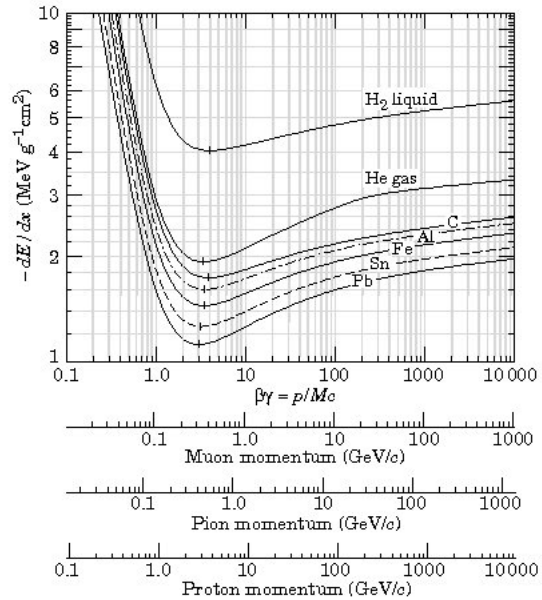


Figure 2.6: Mean energy loss rate of gaseous helium and carbon, amongst others [10]. Since the energy loss scales with the atomic number of the absorber divided by the atomic mass, the energy loss curve for argon lies between the curve for helium and carbon.

The addition of small amounts of molecular gases to noble gases which can interact inelastically with the electrons - by rotational or vibrational excitations - can lead to a strong

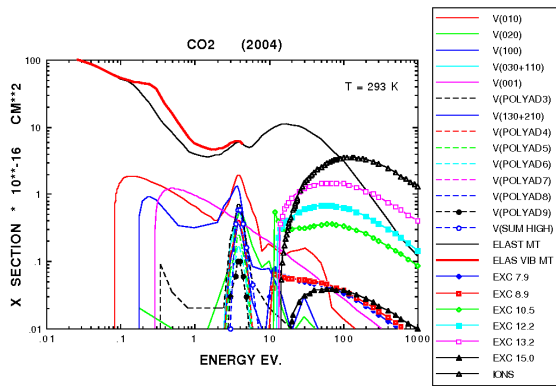


Figure 2.7: Electron cross sections in carbon dioxide [5]

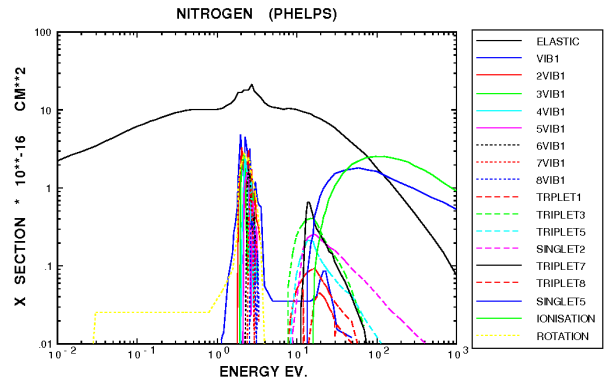


Figure 2.8: Electron cross sections in nitrogen [5]

growth in drift velocity. In the case of inelastic collisions, diffusion is reduced and the electrons drift towards the anode more directly as illustrated in figure 2.9. In a drift tube as studied in this work, this leads to a reduction of the maximum drift time from 4557 ns for pure argon to 448 ns for a gas mixtures containing 3% CO₂ [4].

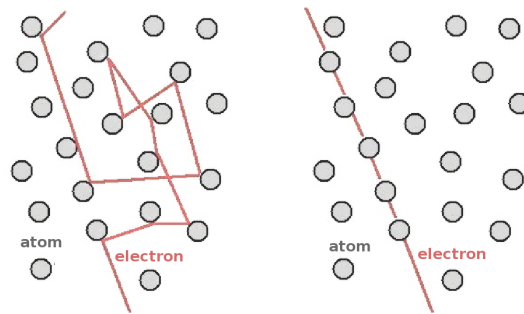


Figure 2.9: Diffusion leads to larger drift times than pure drift. [20] (modified)

Neutralization

Positive ions can be neutralized when recombining with an electron or negative ion of the gas or by extracting an electron of the tube wall.

An electron can be neutralized by recombination with an ion, by attachment to an electronegative molecule or by absorption to the tube wall.

2.2.3 Electrons in Large Electric Fields

In large electric fields of a few kV per cm, electrons can gain enough energy to produce inelastic phenomena as excitation and ionization when colliding with atoms or molecules. Collisions with weakly bound polyatomic molecules lead to radiation-less excitation of rotational and vibrational nature. In case of collisions with noble gases, the excitation occurs through photon absorption or emission making ionization of noble gases likely.

This leads to the phenomena of gas amplification in high electric fields when noble gases are used. In high electric fields the electrons can gain enough kinetic energy to ionize atoms due to collisions. The newly generated electrons can also lead to ionization and so on. This phenomena is called avalanche multiplication. The gas amplification of a gas mixture can be characterized by the *Townsend coefficient*, as will be explained in the following.

The average distance an electron travels before colliding, α , is the mean free path for ionization. The inverse of the mean free path for ionization, α^{-1} , is known as the Townsend coefficient, representing the probability of an ionization per unit path length. For non-uniformal fields like in a cylindrical drift tube the Townsend coefficient depends on the position r inside the tube, $\alpha = \alpha(r)$, the gas amplification factor M is then given by

$$M = \exp\left(\int_{r_1}^{r_2} \alpha(r)^{-1} dr\right) \quad (2.8)$$

for electrons traveling from r_1 to r_2 in the detector.

2.2.4 Cylindrical Counters

The advantage of a cylindrical proportional counter is that gas amplification occurs in a small region around the wire only. In a planar detector with parallel anode and cathode plates, uniformal electric field and gas amplification inside the whole detector, the collected charge depends on the distance of the primary ionization to the anode. In this case, the conclusion from the collected charge to the amount of primary charges is complex. Not so in a cylindrical detector. Only very close to the anode wire where the electric field increases rapidly with r^{-1} , the electrons get multiplied, regardless to where the primary ionization occurred.

Figure 2.10 shows the dependence of the collected charge on the potential difference between anode and cathode. The following explains the different operation modes of detectors with reference to figure 2.10.

Recombination before collection (I): At 0 Voltage all electron-ion pairs generated by the passing radiation recombine under their electrical attraction. At small voltages, some charge is collected, but recombination is still the dominant process.

Ionization Chamber (II): Increasing the voltage, more and more pairs are collected before they can recombine. At some point an increase in voltage shows no effect since all

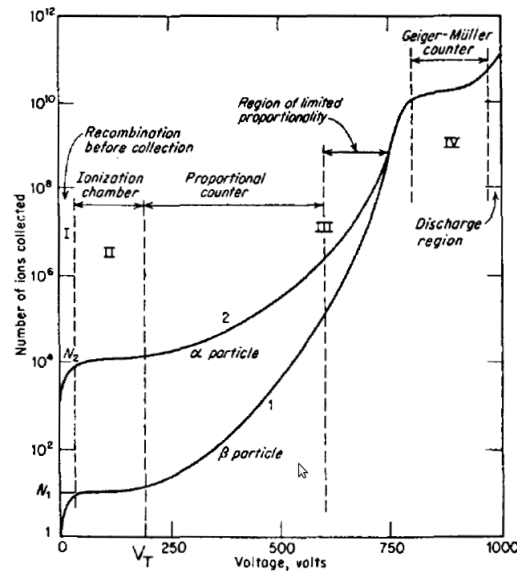


Figure 2.10: Different operation modes of cylindrical counters [25]. The collected charge depends on the applied voltage.

pairs are collected. However, the signal is still small. A detector working in this mode is called Ionization Chamber.

Proportional Chamber ($< \text{III}$): If the voltage is increased above V_T , then the electric field near the anode is high enough for the multiplication process. The primary electrons reaching the anode region are amplified in a way that the collected charge is directly proportional to the primary charge.

Limited Proportionality ($> \text{III}$): At voltages beyond point III, proportionality is lost due to electric field distortions as a consequence of space charge effect. The operation in this region is called streamer mode.

Geiger-Müller Counter (IV): For even higher voltages, photons emitted by deexciting molecules travel through the medium, leading to chain reactions of avalanches along the total length of the anode wire. The collected current is then saturated and the signal is independent of the initial ionizing event. The detector now works in Geiger-Müller operation. Higher voltages could lead to a continuous breakdown regardless if radiation was seen or not. This region has to be avoided in order to prevent the detector from damage.

2.3 Problems with Ar:CO₂ 93:7

To clarify the motivation for drift gas studies, figure 2.11, shows the spatial resolution of ATLAS muon chambers under different radiation levels, which was studied by M. Deile et al [13]. The following will explain the reason for the deterioration of the resolution under irradiation for large radii.

Due to irradiation, space charge effects arise inside the tube medium. When the positive ions, which show a smaller velocity than the electrons, drift towards the cathode, the electric field is changed. Figure 2.12 shows the drift velocity of electrons against the electric field. The drift velocity was simulated using GARFIELD [4]. As can be seen, the drift velocity varies with the electric field. If the electric field is now changed due to ions, then the drift velocity of electrons arising from an actual muon event is influenced. However, the translation from drift time to drift radius is done for all events using the same rt-relation, leading to a decrease in resolution if space charges affect the electric field.

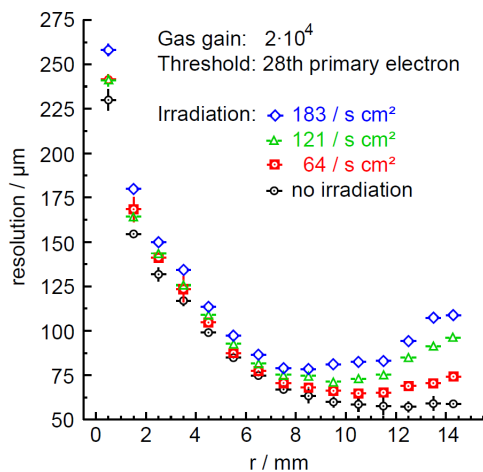


Figure 2.11: Spatial resolution of ATLAS muon chambers under different irradiation levels [13]

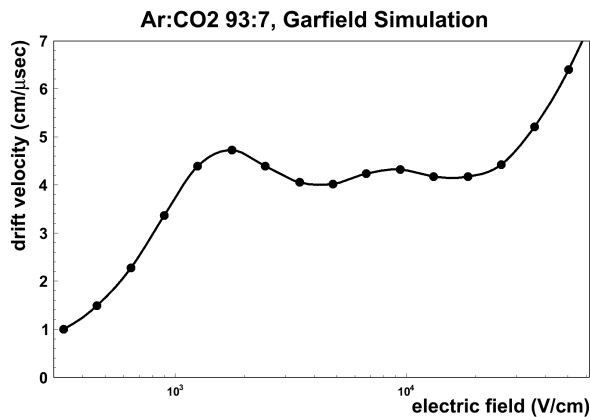


Figure 2.12: Simulated drift velocity inside a drift tube against electric field.

2.4 Requirements for Drift Gases

One of the most critical choices concerning the working parameters of the MDT chambers is the choice of the drift gas. The following points display the properties of an optimized drift gas with respect to high luminosity at LHC. A detailed description on the selection of the currently used gas mixture Ar:CO₂ 93:7 can be found in [7].

- **Fast Drift Gas:** After passage of an ionizing particle, a drift tube filled with Ar:CO₂ 93:7, with a maximum drift time of 700 ns, might be occupied for 700 ns. At high background rates a drift tube is strongly occupied by background signals. Since this occupancy is proportional to the maximum drift time, faster gas mixtures with small maximum drift times are essential for reducing the occupancy. The efficiency of one MDT tube without background rate has to be $\geq 99\%$.
- **Linear RT-Relation:** As explained in 2.3, a linear rt-relation is important in order to reduce the negative impact of space charge effects on the resolution. A drift velocity independent of the electric field is desirable.
- **Gas Amplification:** The ATLAS Muon Chambers are to operate at gas gain $2 \cdot 10^4$. Gas amplification is required in order to distinguish the muon signal from noise or background events.
- **Small Afterpulsing:** Some gas mixtures show afterpulsing. This means that there are still electrons collected at the wire after the maximum drift time. A physical explanation for this effect are photons which are generated during the gas amplification process when electrons and ions recombine or when an excited atom de-excites. These photons can then lead to photo effect at the tube wall creating electrons. A more detailed explication is given in section 4.7.3. The afterpulsing is desired to be small since it enlarges the occupancy and may contribute to aging effects.
- **No Ageing Effects:** Potential to replacement of hardware is to be avoided and therefore the MDT chambers must operate stable as long as possible. Therefore, ageing effects must be eliminated. For this reason, only gases that do not create depositions on the wire can be used. For example studies of CH₄ have shown increasing ageing effects [8]. Favorable gases are inert gases as all noble gases, nitrogen and carbon dioxide. Gas mixtures containing tetrafluoromethane Ar:CF₄ 93:7, Ar:CF₄ 95:5, Ar:CF₄ 90:10 and Ar:CF₄ 80:20 have been studied in [18] and showed large afterpulsing for the mixtures with CF₄ $\leq 10\%$ contents. Large contents of CF₄ however are not desirable because of the aggressive Fluor generated by CF₄ decomposition.
- **Large Atomic Number:** The number of ionized particles due to the passing radiation gives information on the energy of the through-going particle. Gases with large atomic numbers lead to more primary ionization and are therefore preferable in order to obtain sufficiently large signals, but are also more prone to photo effect.

- **Quenching Properties:** In order to absorb photons, the gas mixture should contain molecules with non-radiative states. Such gases are most organic compounds of the hydrocarbon and alcohol families. Furthermore some inorganic compounds CO_2 and BF_3 .
- **Streamer Rate:** Operation in streamer mode is not desired for the MDT chambers to prevent large amounts of charges from reaching the wire, insuring a long life time for the tubes. Thus the streamer rate should be smaller than 1%. The streamer rate for Ar: CO_2 93:7 was measured to be $< 0.1\%$ for gas gains up to $4 \cdot 10^4$ [7].
- **Lorentz Angle:** The drift gas is supposed to have an rt -relation with a small dependence on the magnetic field. Thus, small Lorentz angles are preferable. The influence of magnetic fields on the electron drift is not treated in this work.

This thesis will treat gas mixtures containing the inert gases argon, carbon dioxide and nitrogen and will investigate different composition ratios of these gases.

Chapter 3

Simulations

In section 2.4 the requirements of an optimized drift gas are presented. This chapter will focus on simulations, in order to find fast gas mixtures with constant drift velocities and linear rt -relations, which is preferable for high luminosities at LHC. In order to understand the individual effect of argon (Ar), carbon dioxide (CO₂) and nitrogen (N₂), the electron drift velocities and rt -relations are simulated for various gas mixtures with different ratios of Ar, CO₂ and N₂ using MAGBOLTZ [5] interfaced to GARFIELD [4]. MAGBOLTZ is a program package which simulates the electron transport properties of various gas mixtures by solving the Boltzmann transport equations for electrons in gas mixtures under the influence of electric and magnetic fields. The program package GARFIELD then uses the electron transport properties for simulating two- and three-dimensional drift chambers.

The simulation results are presented in the following sections. Section 3.1 investigates simulated electron drift velocities, section 3.2 the linearity of simulated rt -relations and section 3.3 the maximum drift times gained from the simulated rt -relations. Finally, the influence of different anode voltages is studied in section 3.4. The presented simulated gas mixtures contain between 90% and 99% argon, between 1% and 10% carbon dioxide and between 0% and 3% nitrogen gas. Table 3.1 displays the parameters used throughout all simulations. No magnetic field was taken into account.

inner tube radius	1.46 cm
wire radius	0.0025 cm
temperature	21.3 °C
pressure	3 bar
ion mobility	$0.5 \frac{cm^2}{Vs}$
voltage at wall	0 V
voltage at wire	3080 V (if not given otherwise)

Table 3.1: Parameters used for simulations

3.1 Drift Velocity

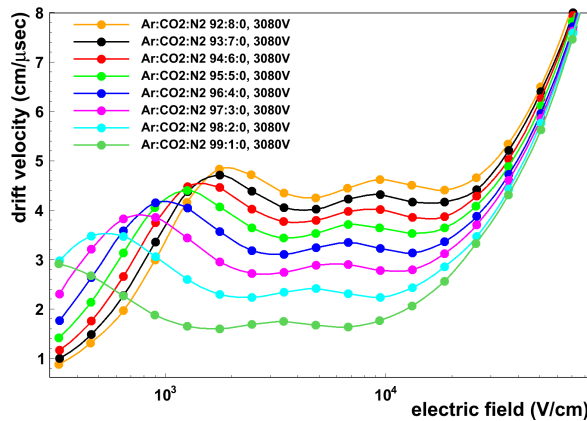


Figure 3.1: Simulated drift velocities against electric field under variation of Ar:CO₂ at 3080 V. N₂ content at 0%. CO₂ content varies between 8% and 1%. The velocity gets less dependent on the electric for smaller CO₂ contents.

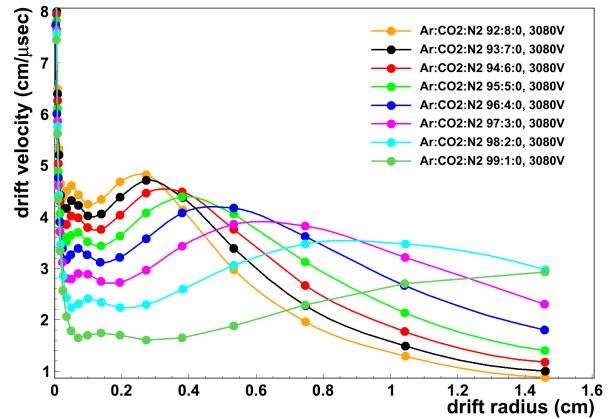


Figure 3.2: Simulated drift velocities against drift radius under variation of Ar:CO₂ at 3080 V. N₂ content at 0%. CO₂ content varies between 8% and 1%. The velocity gets more constant for smaller CO₂ until 2% CO₂.

At first the effect of different Ar and CO₂ ratios on the drift velocity is studied, therefore only gas mixtures without N₂ are presented. In the following figures the points are simulations and the lines are drawn to guide the eye. Simulated velocities for gas mixtures containing CO₂ contents between 1% and 8% and Ar contents between 92% and 99% are plotted against the electric field, figure 3.1, and against the drift radius, figure 3.2.

The black curve in figure 3.1 shows that the drift velocity of the standard gas mixture Ar:CO₂ 93:7 is not constant for all electric fields, but has a small velocity at small electric fields of $E \leq 10^3 \frac{\text{V}}{\text{cm}}$ and a large velocity at higher electric fields of $E > 10^3 \frac{\text{V}}{\text{cm}}$. The simulated drift velocities for gas mixtures with reduced CO₂ contents show, that CO₂ reduction increases the drift velocities at small electric fields, and decreases them at larger fields. The reduction of the CO₂ content down to about 2% - 3% leads to more constant velocities. Beyond, the non-linearity increases again. Gas mixtures with e.g. 2% and 3% CO₂ are fast, as for drift radii above 0.5 cm the velocities are larger than for the standard gas mixture, and show more constant velocities.

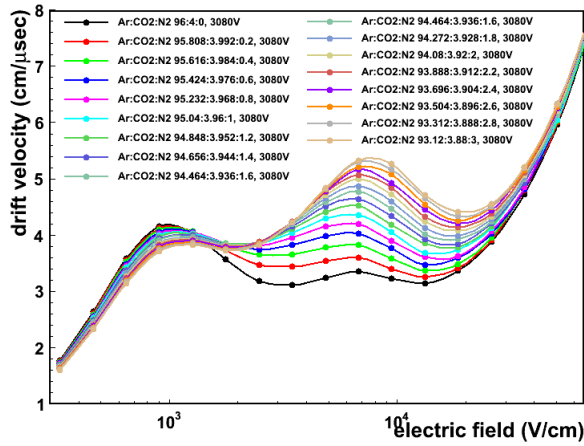


Figure 3.3: Simulated drift velocities against electric field with fixed ratio Ar:CO₂ 96:4 and addition of up to 3% N₂. The velocity gets less dependent on the electric field for small N₂ contents of around 1%.

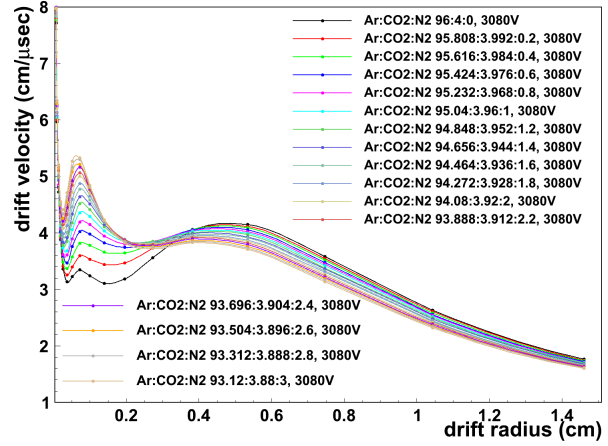


Figure 3.4: Simulated drift velocities against electric field with fixed ratio Ar:CO₂ 96:4 and addition of up to 3% N₂. The velocity gets more constant for small N₂ contents of around 1%.

In the following the influence of small amounts of N₂ on the drift velocity is studied. For this purpose, the Ar:CO₂ ratio is left at a constant ratio of 96:4 and amounts of N₂ ranging from 0% to 3% are added to the gas mixture. The simulation results are shown in figure 3.3 and 3.4.

At small electric fields, the addition of N₂ shows no large impact on the drift velocity. However at fields between $1.1 \cdot 10^3 \frac{\text{V}}{\text{cm}}$ and $1.1 \cdot 10^4 \frac{\text{V}}{\text{cm}}$, the velocity increases for larger N₂ values. At 3% N₂ the velocity is 60% larger than at 0% N₂. The velocity increase at high electric fields for N₂ addition is also observed by Avramidou et al. [9].

From Figures 3.3 and 3.4 it seems, that the addition of about 1% N₂ leads to more constant drift velocities. Thus, gas mixtures containing 1% of N₂ and CO₂ contents between 0%

and 9% are shown in 3.5 and 3.6. Linear and fast gas mixtures are e.g. Ar:CO₂:N₂ 95:4:1, 96:3:1 and 97:2:1. However, a more quantitative study on the linearity is presented in the following.

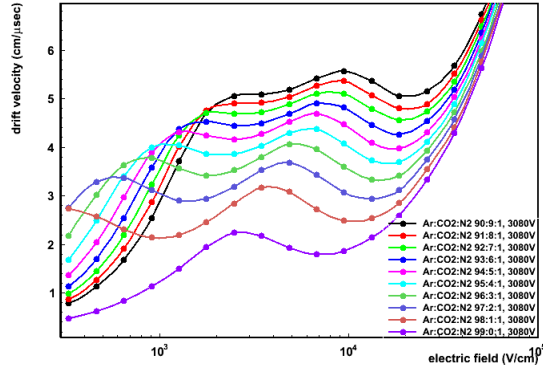


Figure 3.5: Simulated drift velocities against electric field with fixed N₂ content of 1% and varying of CO₂ contents from 0% to 9%. Gas mixtures with small velocity dependence on the electric field are e.g. Ar:CO₂:N₂ 95:4:1, 96:3:1 and 97:2:1

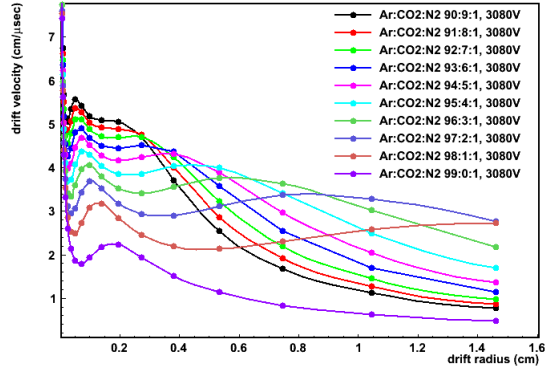


Figure 3.6: Simulated drift velocities against drift radius with fixed N₂ content of 1% and variation CO₂ contents from 0% to 9%. Gas mixtures with constant drift velocities are e.g. Ar:CO₂:N₂ 95:4:1, 96:3:1 and 97:2:1

3.2 Linearity

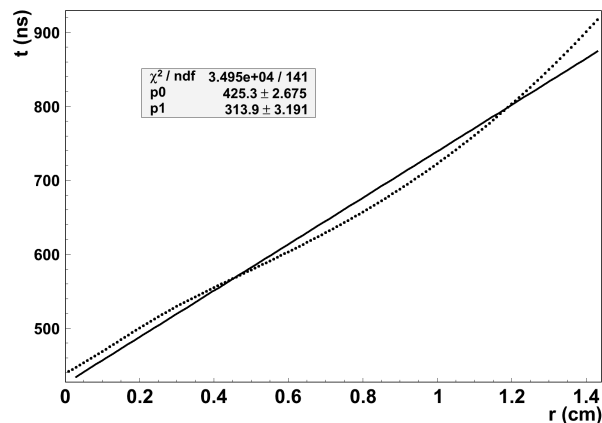


Figure 3.7: Measure for linearity: $\frac{\chi^2}{\text{ndf}}$ of a linear fit (line) to the rt -relation (dots)

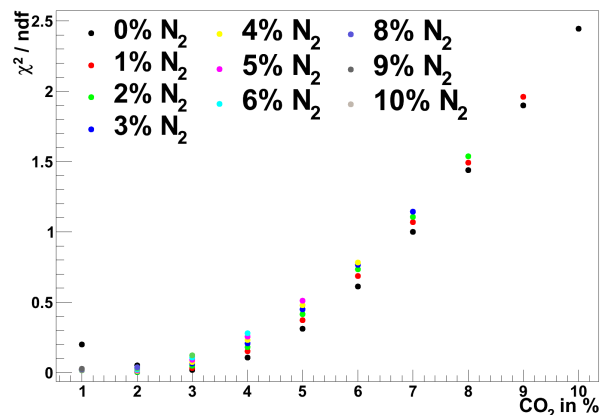


Figure 3.8: $\frac{\chi^2}{\text{ndf}}$ for CO_2 between 1% and 10% and N_2 between 0% and 10%. The most linear gas mixtures are around 2% CO_2 . At 1% CO_2 the data points for 1% - 10% N_2 are all hidden behind the purple point around 0.02 $\frac{\chi^2}{\text{ndf}}$.

The rt -relation gives information on two important drift properties of a gas mixture: the linearity and the maximum drift time. Therefore, the rt -relation is simulated for various gas mixtures and analysed in terms of linearity and maximum drift time. In this section the results on linearity will be given, in the following section the results on the maximum drift time.

To obtain a measure of the linearity of a gas mixture, a linear function with fit parameters a and b is fitted to the rt -relations, as shown in figure 3.7.

$$t = a + b \cdot r \quad (3.1)$$

The χ^2 divided by the number of degrees of freedom (ndf) then serves as a measure for the linearity of a gas mixture.

Rt -relations for gas mixtures containing between 1% and 10% CO_2 , between 0% and 10% N_2 and between 90% and 100% Ar are simulated. Figure 3.8 shows $\frac{\chi^2}{\text{ndf}}$ of the linear fit against the CO_2 content. The N_2 content is encoded in colours. The sum of $\text{Ar}\% + \text{CO}_2\% + \text{N}_2\%$ equals 100%. Starting from the standard gas mixture Ar: CO_2 93:7 the linearity increases - meaning that $\frac{\chi^2}{\text{ndf}}$ decreases - for less CO_2 contents. The most linear gas mixtures are at 2% CO_2 . Furthermore the addition of N_2 has a smaller impact on the linearity than CO_2 .

For CO_2 larger than 2%, N_2 has a negative influence on the linearity, for $\text{CO}_2 \leq 2\%$ the influence of N_2 is positive.

In order to study the effect of N_2 in more detail, a certain ratio of $\text{Ar}:\text{CO}_2$ was kept fixed and amounts of N_2 ranging from 0% to 3% were added. The results are shown in figure 3.9 and 3.10. The linearity decreases for most gas mixtures at the addition of N_2 . However, for 1% and 2% CO_2 $\frac{\chi^2}{\text{ndf}}$ is minimal at 1.4% and 1.2% N_2 respectively (figure 3.10) and shows therefore an improvement in linearity for small CO_2 contents of 1% and 2%.

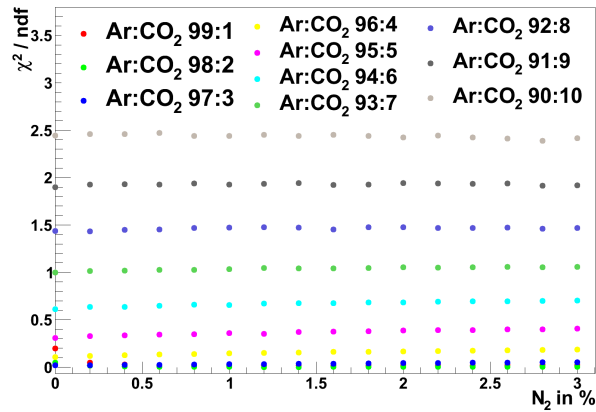


Figure 3.9: $\frac{\chi^2}{\text{ndf}}$ for different fixed $\text{Ar}:\text{CO}_2$ contents. Addition of N_2 of up to 3%. CO_2 varies between 1% and 10%. The red points for 1% CO_2 are hidden behind the blue and green points for 2% and 3% CO_2 . A zoomed view of this region is shown on the right in figure 3.10.

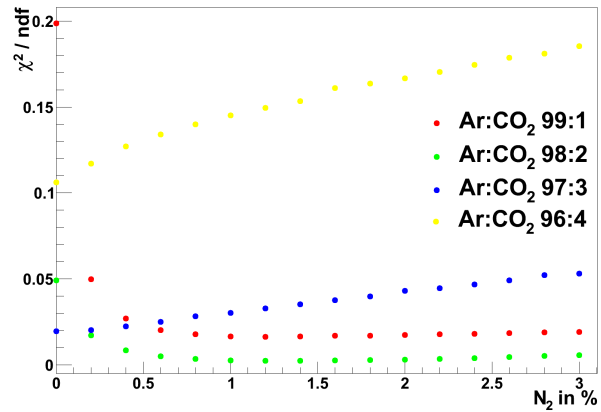


Figure 3.10: $\frac{\chi^2}{\text{ndf}}$ for different fixed $\text{Ar}:\text{CO}_2$ contents under the addition of N_2 up to 3%. CO_2 varies between 1% and 4%. For CO_2 contents of 1% and 2% small N_2 addition of up to 1.4% and 1.2% N_2 , respectively, leads to improvement in linearity.

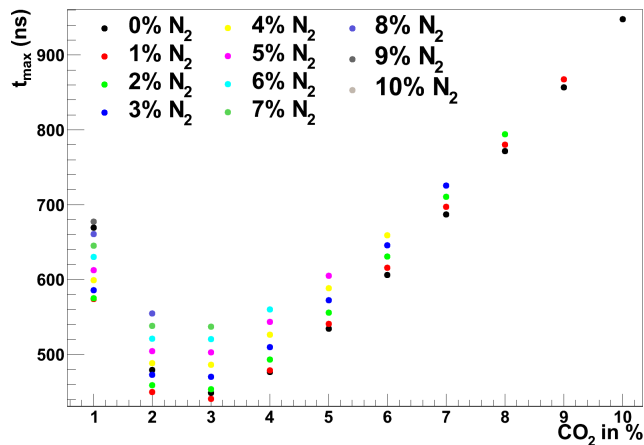


Figure 3.11: Simulated maximum drift times for CO_2 between 1% and 10% and N_2 between 0% and 10%. Fastest gas mixtures contain 3% CO_2 . For $\text{CO}_2 \leq 4\%$ the addition of N_2 up to a certain amount minimizes the maximum drift time.

3.3 Maximum Drift Time

The maximum drift time is obtained by the simulated rt -relations. As value for the *maximum drift time*, the value for the drift time at the largest drift radius, 1.43 cm, given by the rt -relation, is taken. Figure 3.11 shows the maximum drift times for CO_2 contents between 1% and 10%, N_2 contents between 0% and 10% and Ar contents between 90% and 100%.

There is a minimum of the maximum drift time at 3% CO_2 for all gas mixtures with equal N_2 content. For gas mixtures with CO_2 contents larger than 3% the addition of N_2 has a negative impact on the maximum drift time. For gas mixtures with CO_2 contents $\leq 3\%$, small amounts of N_2 reduce the maximum drift time.

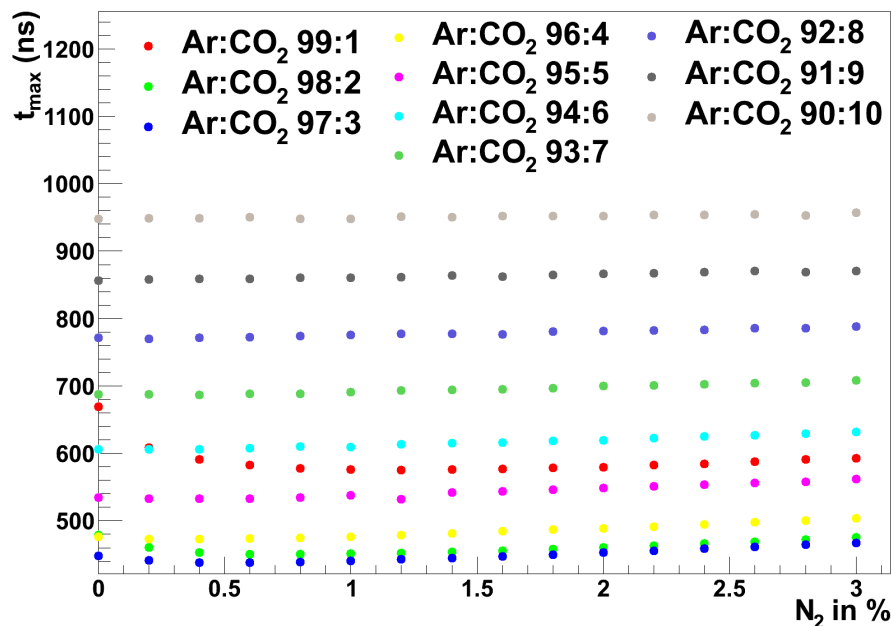


Figure 3.12: Simulated maximum drift times for different fixed Ar:CO₂ ratios and addition of N₂ up to 3%. CO₂ contents between 1% and 10%. A zoom of the region $t_{max} < 670ns$ is given in figure 3.13.

Figure 3.12 and 3.13 illustrate the maximum drift times for various constant Ar:CO₂ ratios from 100:0 to 90:10 and N₂ contents between 0% and 3%. Table 3.2 gives for each Ar:CO₂ ratio the corresponding N₂ content where the maximum drift time is at a minimum. At smaller CO₂ contents a larger amount of N₂ minimizes the drift time, for example 1.2% N₂ at 1% CO₂. At larger CO₂ contents only a small N₂ content shows a positive effect.

Table 3.2: N₂ minima of t_{max} for constant Ar:CO₂ ratios as in figure 3.13

CO ₂	1	2	3	4	5	6	7	8	9	10
N ₂	1.2	0.8	0.6	0.4	0.4	0.4	0.4	0.2	0	0

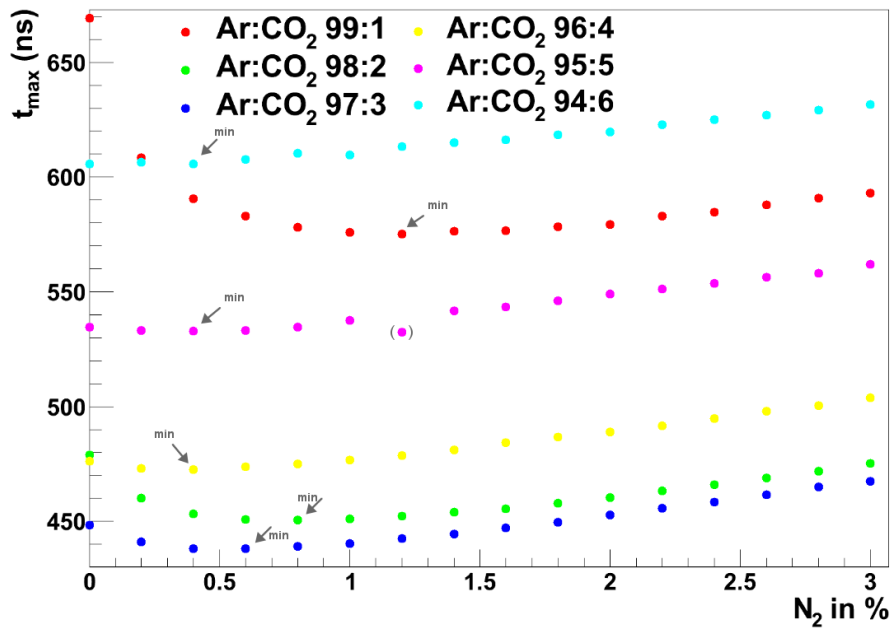


Figure 3.13: Zoom of figure 3.12 for $t_{max} < 670$ ns. Simulated maximum drift times for different fixed Ar:CO₂ ratios and addition of N₂ up to 3%. CO₂ contents between 1% and 6%. The fastest gas mixtures contain 3% CO₂. Maximum drift times below 450 ns are achievable. The addition of small amounts of N₂ decreases the maximum drift times.

3.4 Influence of the Anode Voltage

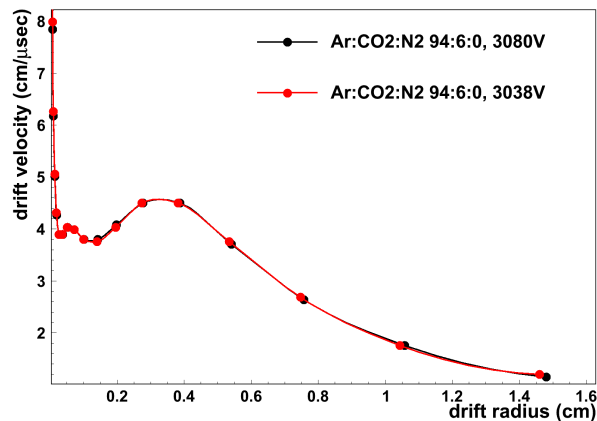


Figure 3.14: Drift velocity of Ar:CO₂:N₂ 94:6:0 at 3038 V and 3080 V

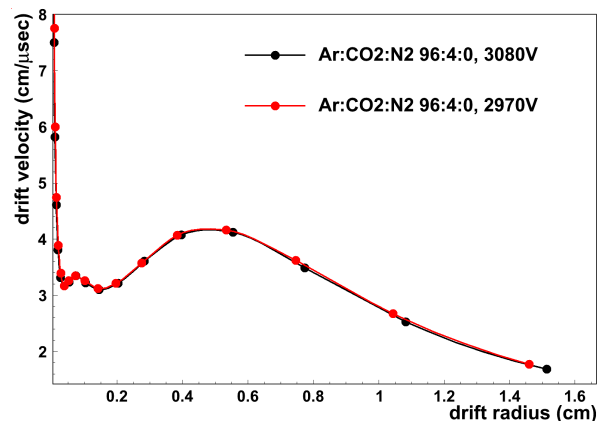


Figure 3.15: Drift velocity of Ar:CO₂:N₂ 96:4:0 at 2970 V and 3080 V

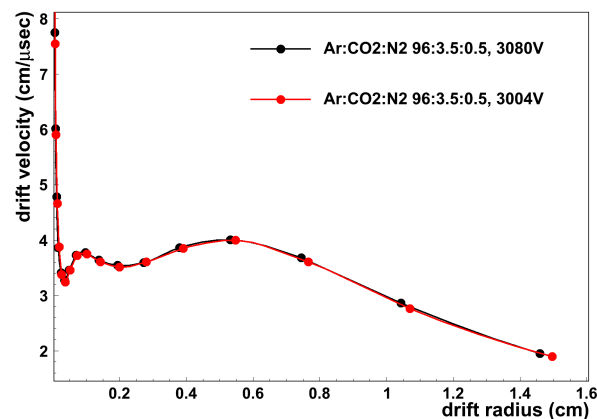


Figure 3.16: Drift velocity of Ar:CO₂:N₂ 96:3.5:0.5 at 3004 V and 3080 V

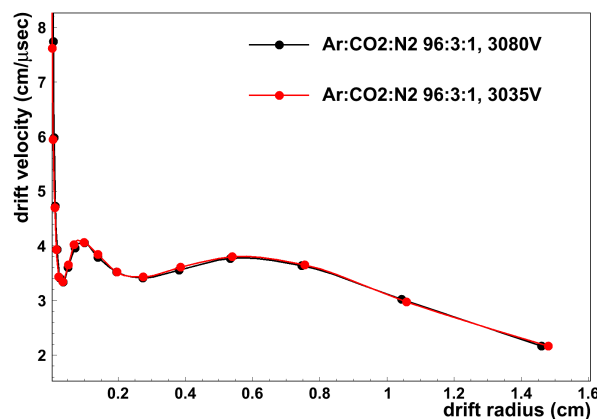


Figure 3.17: Drift velocity of Ar:CO₂:N₂ 96:3:1 at 3035 V and 3080 V

In the following the influence of different high voltages at the anode on the drift velocity will be studied. Figures 3.14 - 3.17 show simulated drift velocities for the gas mixtures Ar:CO₂:N₂ 94:6:0, 96:4:0, 96:3.5:0.5 and 96:3:1 against the drift radius. For each gas mixture the drift velocity for 3080 V is compared to the drift velocity at a smaller voltage. The smaller voltage is chosen in order to achieve a gas gain of approximately 20 000. The voltage values were taken from measurement results as described in the next chapter section 4.8 showed. The simulation shows, that there is no significant change in drift velocity within the studied voltage range.

3.5 Summary

The most linear gas mixtures contain between 1% and 3% CO₂. For 1% and 2% CO₂, the addition of small amounts of N₂ up to 1.5% is preferable. Fast gas mixtures contain between 2% and 4% CO₂. Additional small amounts of N₂ up to 1.2% show a positive effect on the maximum drift time. The studied reduction of the anode voltage from 3080 V to minimally 2970 V, did not show significant changes in the drift velocity.

Chapter 4

Experimental Results for Ar:CO₂ and Ar:CO₂:N₂ Gas Mixtures

Gas mixtures containing Ar, CO₂ and N₂ were tested in an experimental set-up consisting of ATLAS drift tubes using cosmic muons. The measurements were analyzed and the gas mixtures characterized with regard to the drift gas requirements of section 2.4.

This chapter will present the experimental set-up, the data acquisition and the methods used for the data analysis. Furthermore, the experimental results will be presented.

4.1 Experimental Set-Up

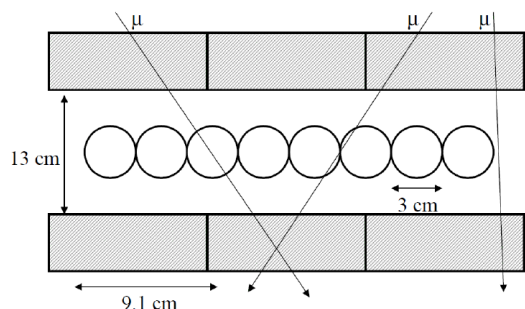


Figure 4.1: Experimental set-up: 8 ATLAS BOS drift tubes, 4 m long, scintillators as triggers on top and bottom and on both ends of the drift tubes, cosmic muons [28]

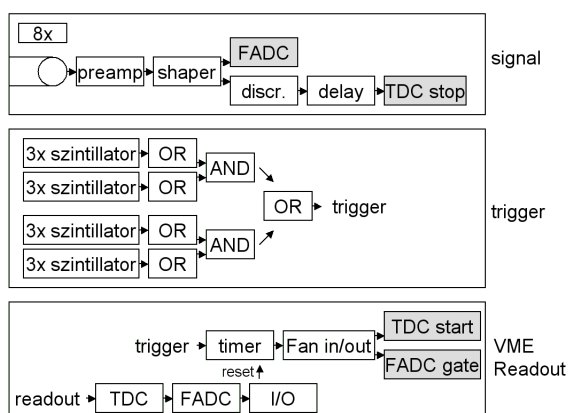


Figure 4.2: Schematic readout and trigger logic [28]

Figure 4.1 shows a cross section of the experimental set-up. It consists of 8 ATLAS standard **Barrel Outer Small (BOS)** drift tubes of 4 m length and 3 cm diameter. The tube wall consists of aluminum of 0.4 mm thickness. Centrally in the tube a tensioned tungsten-rhenium wire of 50 μm diameter is at high voltage. The tubes are sandwiched between two layers of scintillators which act as triggers on cosmic muons. Different gas mixtures can be introduced into the tubes with the help of a gas mixing system which is also responsible for the stabilization of the pressure to 3 bar.

The trigger schedule and readout system are shown schematically in figure 4.2. The trigger system on cosmic muons consists of scintillators that are of 9 cm width and 70 cm length and produce scintillation light after passage of a cosmic muon. A fast coincidence between upper and lower scintillators triggers on through-going muons. There are two such trigger systems one at each end of the tubes.

4.2 Data Acquisition

When a muon passes the set-up, a trigger signal is sent to the *timer* module (see figure 4.2, *VME Readout*). The timer then gives a start signal to the TDC and the Flash-ADC. The signal at the anode wire (see figure 4.2, *signal*) is pre-amplified before passing a shaper and being digitized by a Flash-ADC at 1 GHz sampling rate. The FADC has a ring buffer which allows to record data before the trigger signal. This offset is around 430 ns. In addition, the signal at the wire passes a discriminator which directs it to the TDC. When the signal has reached the TDC, the time between trigger signal and discriminator signal is determined. This time corresponds to the time the fastest electrons need for drifting from their ionization point to the anode wire. Since the trigger signal is delayed due to the signal processing time, the discriminator signal is artificially delayed. The VME-Crate is connected to a PC which stores the recorded data. As soon as the PC has recorded all the data of an event and is ready for more events, it signalizes the time module to enable the next trigger signal.

A typical FADC signal is shown in 4.3. The FADC modules correlate $-0.5\text{ V} \dots +0.5\text{ V}$ to channels $0 \dots 4095$. Consequently channel 2048 represents voltage 0, the baseline. Because of the 430 ns offset of the FADC, the signals with drift time 0 ns start around 430 ns. The event in figure 4.3 has therefore a drift time of 105 ns.

Characteristically for the FADC signal of a muon event is a global maximum at the beginning of the signal. This means, that the greatest number of electrons reach the wire at the beginning of the signal. The reason for this effect gets clear when looking at figure 4.4. All electrons within one circle arrive during the window corresponding to the shaping time Δt . The overlap between a circular segment and the muon track is larger the closer the circle is to the wire. Therefore, the FADC registers more electrons at the beginning of the signal. This effect gets also clear when considering Figure 4.5. Electron clusters near the

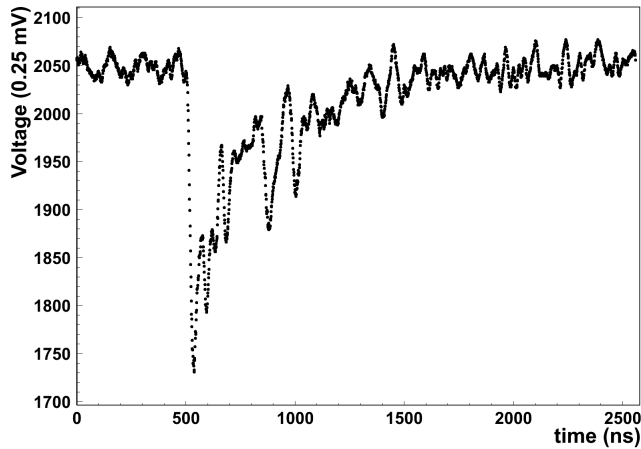


Figure 4.3: Characteristic FADC signal, showing the clustering of the primary electrons due to the non-homogeneous energy-loss of the muons. Because of the 430 ns offset, this event has a drift time of 105 ns.

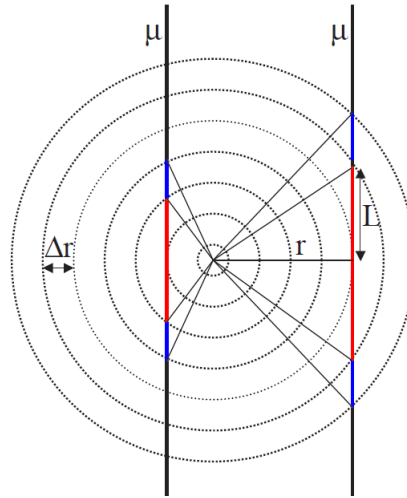


Figure 4.4: Signal generation - geometrical considerations

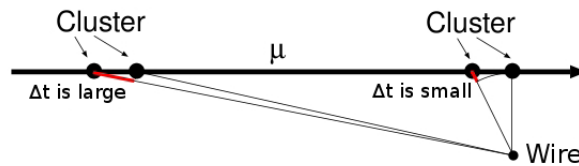


Figure 4.5: Electron cluster close the wire arrive during a short time interval, whereas clusters far from the wire arrive during a large time interval. [18] (modified)

wire arrive during a short time interval, whereas clusters far from the wire arrive during a larger time interval. Therefore, during data acquisition windows at the beginning of the signal more electrons are recorded than during later data acquisition windows.

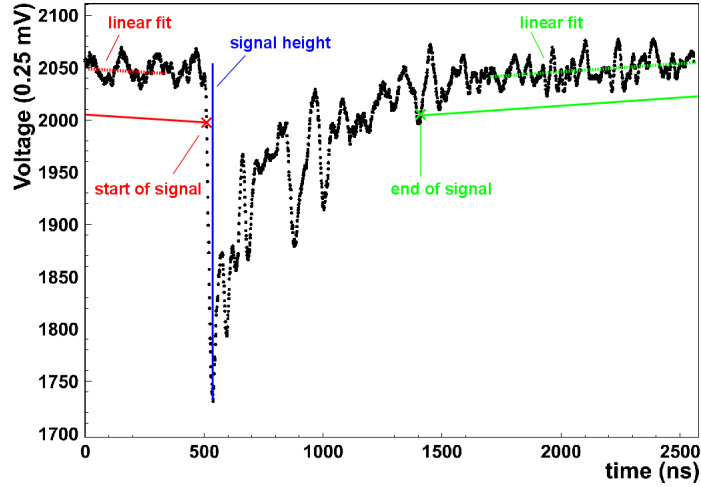


Figure 4.6: Analysis of Flash-ADC signal. 0 V corresponds to channel 2048, the dynamic range of the F-ADC is ± 0.5 V. Details are explained in section 4.3. For $t_{drift} = 0$ ns the signals start around channel 430.

4.3 Data Analysis

Before measurement, a new gas mixture was introduced into the evacuated set-up. At 3 bar absolute pressure the gas was flown for about 10 volume exchanges before taking data. Usually 300000 muon events were recorded within approximately 5.5 h.

To characterize the gas mixtures, the TDC and FADC data were analyzed. Figure 4.6 shows a typical FADC muon event which is analyzed regarding the beginning of the signal, the signal height and the signal end. The analysis is performed by the program *anav3.1.c* which is explained in detail in [28]. After having analyzed a set of events, the program creates amongst others a drift time spectrum, a signal height spectrum, an end of signal spectrum and calculates the rt -relation. In the following it will be briefly explained how these histograms are obtained and how they should look like for an ideal gas mixture.

4.3.1 Drift Time Spectrum

As explained in section 2, the drift time is the time that passes between muon passage and the arrival of the first electrons at the anode. Therefore, the arrival time of the first electrons has to be extracted from the data. This can be done using the TDC or the FADC data.

The TDC determines the time when the signal at the wire crosses a certain threshold set on an external discriminator. The time between the trigger signal and the time obtained by the TDC then corresponds to the time between muon passage and the arrival of the

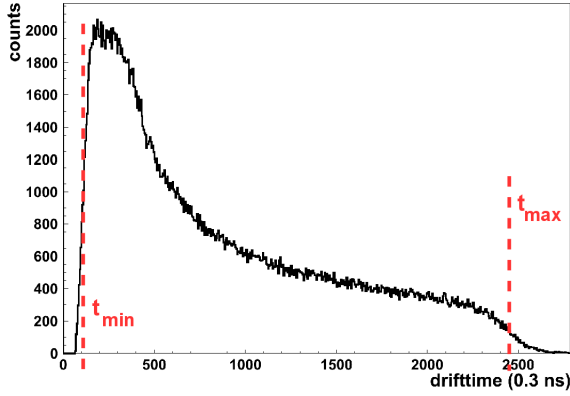


Figure 4.7: Typical TDC drift time spectrum for Ar:CO₂ 93:7, 30000 events

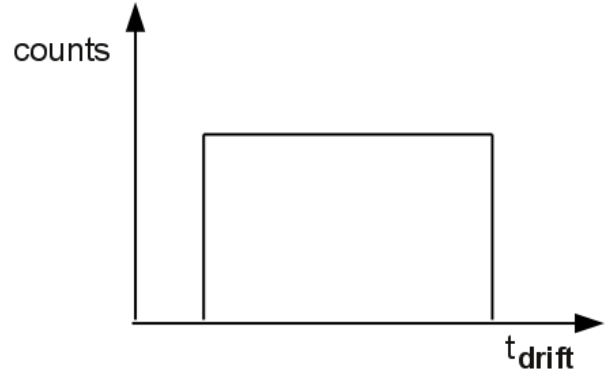


Figure 4.8: Ideal drift time spectrum

first electrons, leading to the so called *TDC drift time*. For a set of events a TDC drift time spectrum can be created.

The drift time can be also obtained by analysing the FADC signal. A linear function is fitted to the base line before the trigger signal. The fit determines the noise level as well. Then a threshold parallel to this linear fit, a little bit above noise, determines the signal start, see “start of signal“ in figure 4.6. The comparison of this time to the trigger signal leads to the *ADC drift time*. This procedure is shown in figure 4.6 in red.

A typical TDC drift time spectrum for Ar:CO₂ 93:7 can be seen in figure 4.7. The drift spectrum gives useful information on a gas mixture, for example on the minimum and maximum drift time, t_{min} and t_{max} which are depicted in red in 4.7, and the drift velocity as will be explained in section 4.3.2. In the following the methods for determining the minimum and maximum drift times will be presented.

There are two methods for determining the minimum and maximum drift time implemented in anav3.1. The *fermi method* fits a fermi function to the rising slope of the drift time spectrum (figure 4.7) and an inverse fermi function to the falling slope with fit parameters a_{min} , t_{min} , T_{min} and a_{max} , t_{max} , T_{max} :

$$\frac{a_{min}}{1 + e^{\frac{t-t_{min}}{T_{min}}}} \quad (4.1)$$

$$a_{max} \cdot \left(1 - \frac{1}{1 + e^{\frac{t-t_{max}}{T_{max}}}}\right) \quad (4.2)$$

as shown in figure 4.9 (green and dark blue curves). The inflexion points (green and dark blue cross in figure 4.9) of these functions, t_{min} and t_{max} , then determine the minimum and

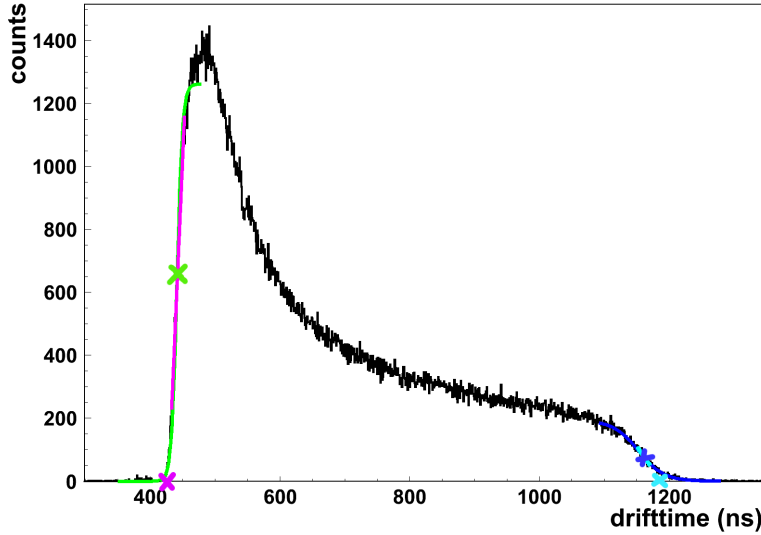


Figure 4.9: Fermi and linear fit to the drift time spectrum for determination of t_{min} and t_{max}

maximum drift time. Fit parameters T_{min} and T_{max} describe the steepness of the rising and the falling slopes.

The *linear fit method* first calculates the derivative of the drift time spectrum to determine the inflexion points of the rising and falling slopes. Then, linear functions are fitted to a symmetrical interval of 10 ns around the obtained inflexion points:

$$0 = a_{min} + b_{min} \cdot t_{min} \quad (4.3)$$

$$0 = a_{max} + b_{max} \cdot t_{max} \quad (4.4)$$

with fit parameters a_{min} , b_{min} , a_{max} and b_{max} , see pink and light blue curve in figure 4.9. The intersection points of the linear fit functions with the x-axis (pink and light blue cross in figure 4.9) then assign the minimum and maximum drift time.

As explained in section 2.4, the drift velocity is preferably constant for all electric fields. An ideal drift velocity is shown in figure 4.10. A constant drift velocity leads to equally distributed drift times, under the assumption that the muons hit the tube homogeneously. The ideal drift time spectrum is therefore box shaped as in figure 4.8.

4.3.2 RT-Relation

We expect every drift radius to be equally probable, since the cosmic muons reach the earth surface homogeneously distributed. However, in the drift time spectrum of Ar:CO₂

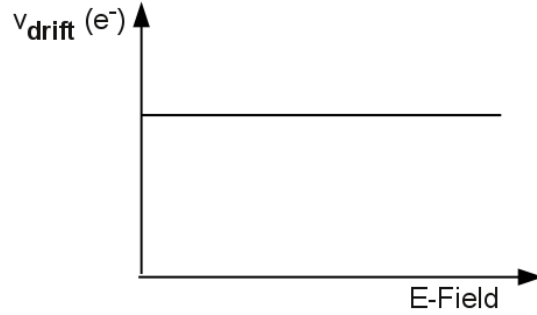


Figure 4.10: Ideal drift velocity

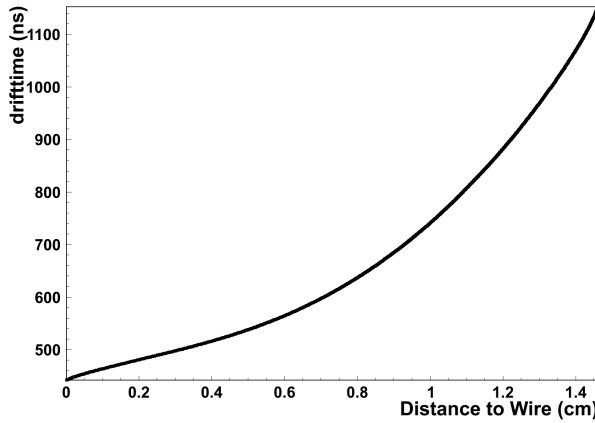


Figure 4.11: Typical rt -relation for Ar:CO₂ 93:7, 30000 events

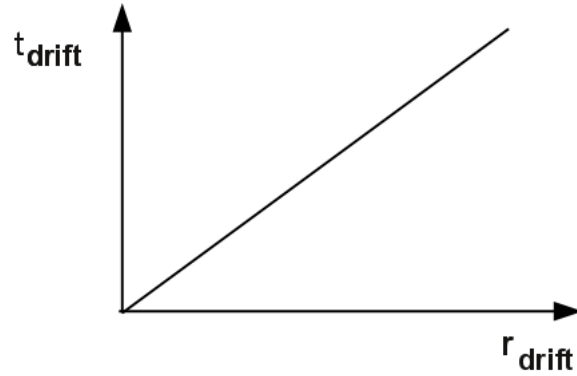


Figure 4.12: Ideal rt -relation

93:7 the drift times are not equally distributed (figure 4.7). In conclusion, the drift time spectrum gives us information about the drift velocity of the gas mixture and hence the space-time-relation, the rt -relation.

The drift velocity can be obtained through the drift time spectrum as follows: If we multiply the drift velocity with $\frac{dN}{dN}$ we obtain equation 4.5.

$$v(t) = \frac{dr(t)}{dt} = \frac{dN(t)}{dN} \frac{dr(t)}{dN} \quad (4.5)$$

Under the assumption that every drift radius is equally probable, $\frac{dr(t)}{dN}$ can be taken as constant, leading to equation 4.6.

$$v(t) = \text{const} \frac{dN(t)}{dt} \quad (4.6)$$

The factor $\frac{dN(t)}{dt}$ can be gained from the drift time spectrum, since every bin of the spectrum

contains the number of events with drift times within Δt . The rt -relation can now be calculated by integrating the drift velocity as in equation 4.7.

$$r(t) = \text{const} \int_{t_{min}}^t \frac{dN(t)}{dt} dt \wedge r(t_{max}) = 14.6 \text{cm} \quad (4.7)$$

The rt -relation now relates the drift radii to the drift times. This relation is important since one can now obtain the drift radius from the measured drift time, which is required for reconstructing the muon track in a chamber with several tube layers. A rt -relation for Ar:CO₂ 93:7 can be seen in figure 4.11.

For an ideal gas mixture with constant drift velocity, the rt -relation is linear, as shown in figure 4.12.

4.3.3 Signal Height

The signal height of a measured event is gained by determining the global minimum of the FADC signal, as shown in figure 4.6. The obtained value is related to the gas amplification of a gas mixture, since a larger gas amplification leads to more electrons reaching the wire and thus to higher signals. In order to study the gas amplification of a gas mixture, signal height spectra are created and analyzed.

Figure 4.13 shows a typical signal height spectrum for Ar:CO₂ 93:7 in logarithmic scale with gas amplification 20 000 at 3080 V. The signal height spectra follow a Landau distribution [21]. The distribution maximum of a gas mixture gives information about the gas amplification when comparing it to the maximum of Ar:CO₂ 93:7 which is at channel 367.

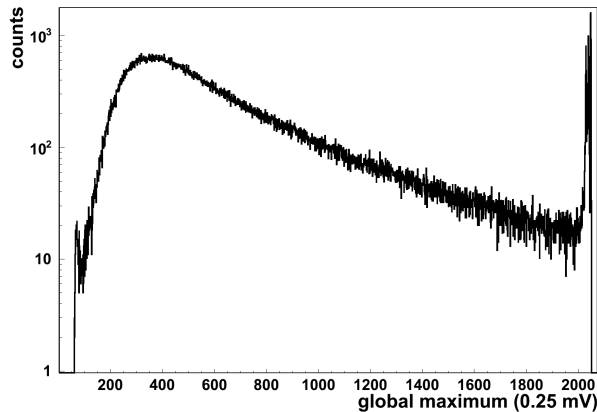


Figure 4.13: Typical signal height spectrum for Ar:CO₂ 93:7, 30000 events in logarithmic scale

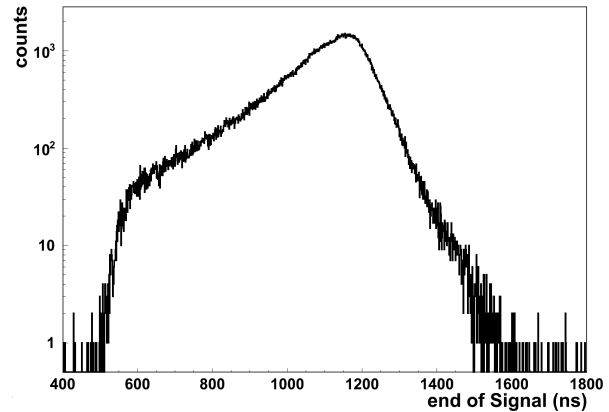


Figure 4.14: Typical end of signal spectrum for Ar:CO₂ 93:7, 30000 events in logarithmic scale

4.3.4 End of Signal

The end of a FADC signal is determined by setting a constant threshold a little bit above a linear fit to the end of a signal (from channel 1500 to 2500) as shown in figure 4.6. The intersection of the threshold and the FADC signal then determines the signal end. A typical end of signal spectrum for Ar:CO₂ 93:7 can be seen in figure 4.14 in logarithmic scale.

The maximum of the signal spectrum corresponds to the maximum drift time. Furthermore, the width of the distribution gives information about the uncertainty of the signal end.

4.3.5 Streamer

In streamer mode the detector works beyond proportional mode leading to high signals (see section 2.2.4). Therefore, large signals are an indication for streamer mode. Thus, the number of large signals, larger than 2020 channels, is investigated for the measured gas mixtures in section 4.8.7. Another sign for operation in streamer mode is the arrival of large amounts of charges which need a long time to discharge. The integral of a signal is proportional to the collected charge. The analysis of the signal integral at late times thus also serves as a measure for streamer signals. The measured gas mixtures are analyzed in terms of integrals after one maximum drift time in 4.7.5 and 4.8.7.

4.4 Results for Ar:CO₂ Gas Mixtures

Starting from the standard gas mixture Ar:CO₂ 93:7, gas mixtures with reduced CO₂ contents from 6% to 3% were measured: Ar:CO₂ 94:6, 95:5, 96:4 and 97:3. The applied high voltage is 3080 V for all gas mixtures.

When comparing the **drift time spectra** of Ar:CO₂ 93:7, 94:6, 95:5, 96:4 and 97:3, figure 4.15, one can see that the drift time spectra get more box shaped the less CO₂ the gas mixture contains. This means that the drift velocity gets more constant the less CO₂ the gas mixture contains, in accordance with the simulations. Furthermore, the drift time spectra end at shorter drift times for less CO₂ fractions, meaning that the maximum drift time - the time that electrons need for drifting from the tube wall to the anode - gets smaller. These results also coincide with the simulation results.

As already seen when analyzing the drift spectra, gas mixtures with reduced CO₂ ratios are faster and more linear. This is also observed in the **rt-relations** which are shown in figure 4.16. Gas mixture Ar:CO₂ 97:3 is the fastest and most linear one. Up to $r = 85$ mm the electron drift time is smaller and above $r = 85$ mm faster than for Ar:CO₂ 93:7.

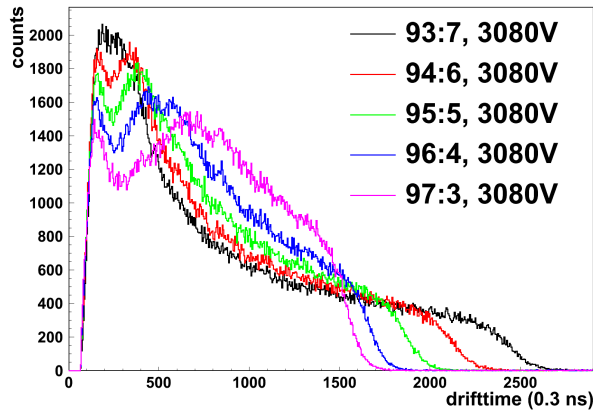


Figure 4.15: Ar:CO₂ gas mixtures - drift time spectra

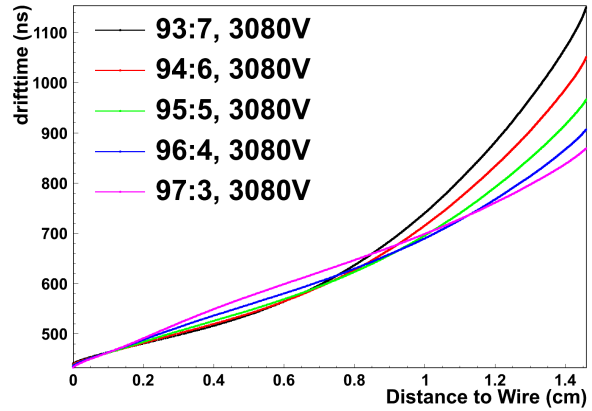


Figure 4.16: Ar:CO₂ gas mixtures - rt-relations

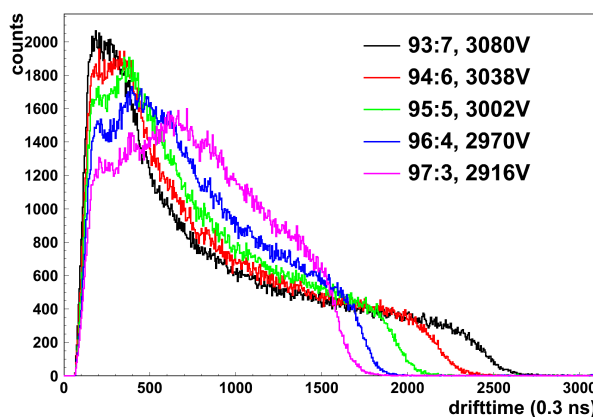


Figure 4.17: Ar:CO₂ gas mixtures - drift time spectra at gas gain 20 000

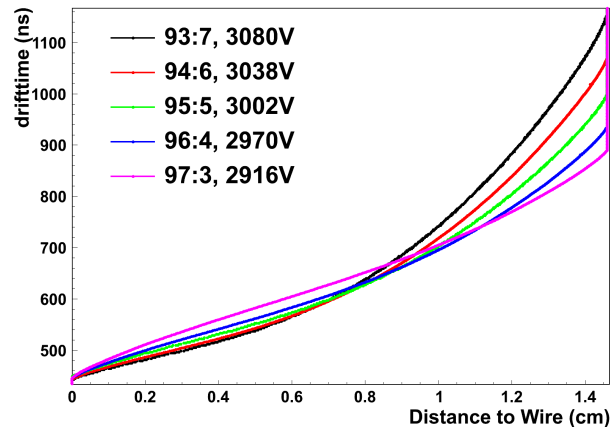


Figure 4.18: Ar:CO₂ gas mixtures - rt-relations at gas gain 20 000

In order to study the gas amplification, the **signal height spectra** are compared in figure 4.19 in logarithmic scale. The maxima of the distributions shift to higher values for smaller CO₂ ratios. Comparing the maxima leads to a gas amplification for Ar:CO₂ 94:6 which is 40.1%, for 95:5 82.9%, for 96:4 127.3% and for 97:4 206% larger than the gas amplification 20 000 for the standard gas mixture.

In figure 4.20 the **end of signal spectra** are shown in logarithmic scale. In accordance with the earlier conclusions, the maxima shift to lower values for smaller CO₂ contents, meaning that the gas mixtures with less CO₂ are faster. Furthermore, the distributions are sharper the less CO₂ the gas mixture contains. But the gas mixtures Ar:CO₂ 94:6, 95:5, 96:4 and 97:3 show shoulders after a maximum drift time in comparison to the standard gas mixture Ar:CO₂ 93:7. All gas mixtures in figure 4.20 end at the same time. This is not observed for all in this work analyzed gas mixtures as is shown later on in figure 4.38.

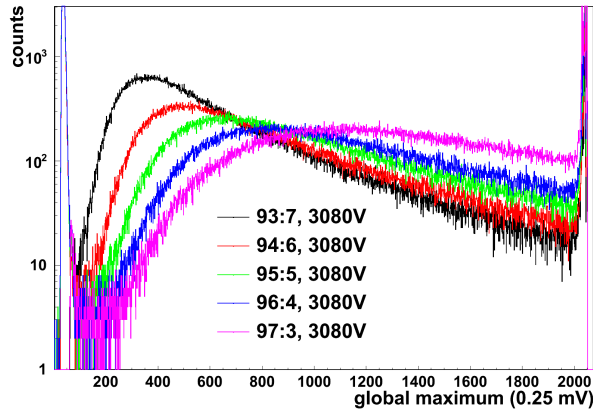


Figure 4.19: Ar:CO₂ gas mixtures - signal height spectra in logarithmic scale

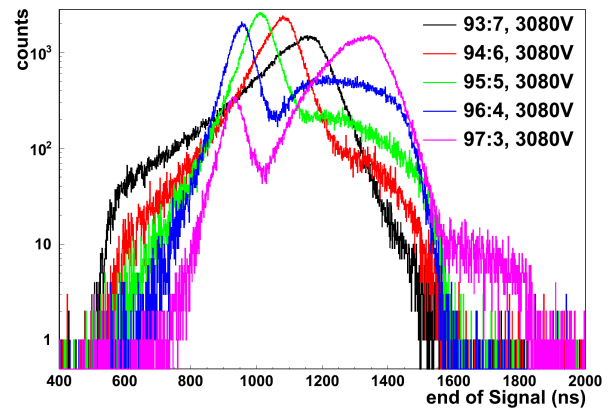


Figure 4.20: Ar:CO₂ gas mixtures - end of signal spectra in logarithmic scale

At the ATLAS detector a gas gain of 20 000 is desired. Therefore, the presented gas mixtures were also measured with reduced voltages at gas gain 20 000. Furthermore, since the analysis of the FADC signals leads to a better comparison if the gas mixtures have signals with same heights, the comparison of gas mixtures at same gas gain is more adequate. As expected, the signal height spectra of Ar:CO₂ gas mixtures are similar, see figure 4.21. This allows a better comparison of the end of signal spectra, as shown in figure 4.22. Gas mixtures with small CO₂ contents still show small shoulders, however considerably reduced in comparison to 3080 V. The drift time spectra and rt-relations for the gas mixtures at gas gain 20 000 are shown in figure 4.17 and 4.18.

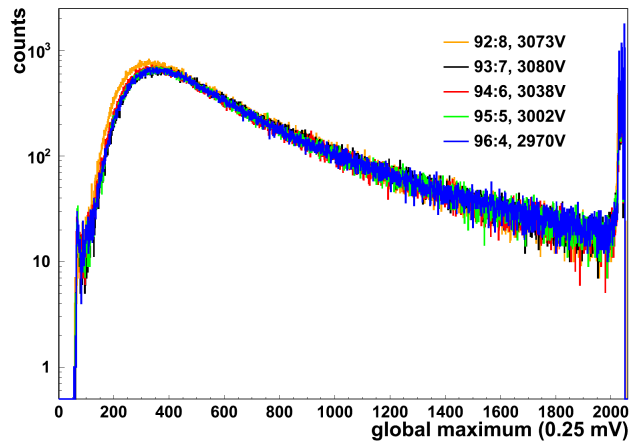


Figure 4.21: Ar:CO₂ gas mixtures at gas amplification 20 000 - signal height spectra

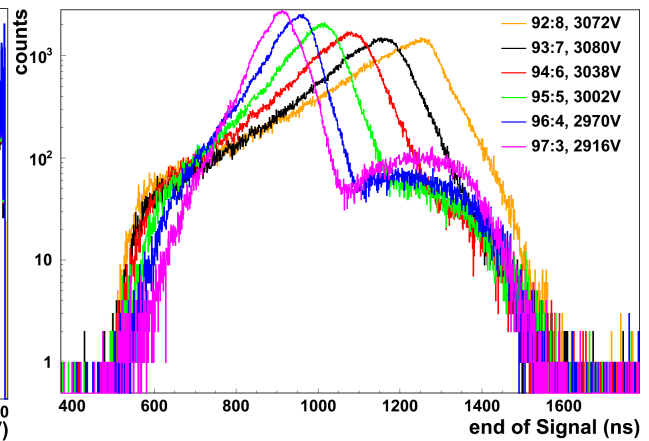


Figure 4.22: Ar:CO₂ gas mixtures at gas amplification 20 000 - end of signal spectra

A further investigation of the end of signal distribution will be given in section 4.7.2. Before that, the influence of the operation at different voltages will be investigated in the next section.

4.5 Operation at Different Voltages

Figure 4.19 shows that the variation of the Ar and CO₂ contents affects the gas gain. To study the consequence of different gas gains on the drift properties of a gas, we will look at one gas mixture operated at two different voltages. As example the gas mixture Ar: CO₂ 96:4 at 2970 V and 3080 V will be compared.

4.5.1 Drift Time Spectrum and RT-Relation

Comparing the **drift time spectra**, figure 4.23, one can see that for 2970 V the spectrum is slightly longer than for 3080 V. Moreover, the rise at small drift times is faster for 3080 V.

The **rt-relation**, figure 4.24, is slightly more linear for 3080 V.

Concluding, the gas mixture is faster and more linear at a higher voltage, but the differences are only small.

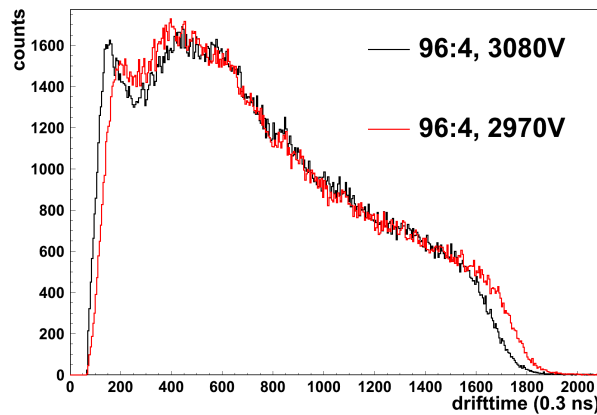


Figure 4.23: Ar:CO₂ 96:4 at 3080 V and 2970 V - comparison of drift time spectra

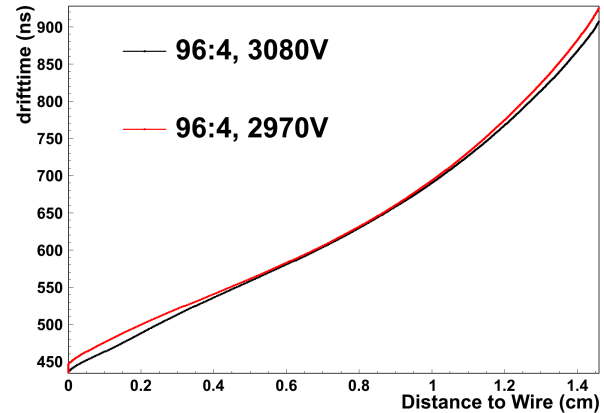


Figure 4.24: Ar:CO₂ 96:4 at 3080 V and 2970 V - comparison of rt-relations

4.5.2 Signal Height and End of Signal

In figure 4.25, the maximum of the signal height spectrum shifts to a significant higher value at 3080 V. The reason for this is that the gas amplification increases for higher anode

voltages. At 2970 V the maximum of the global maximum spectrum is at the same value in comparison to the standard gas mixture 93:7 at 3080 V, meaning that the gas amplification for 96:4 at 2970 V is around 20 000. In figure 4.26 signal heights for averaged FADC signals for different drift times are shown (the averaged FADC signals are explained in 4.7.1). The signals are by more than a factor of 2 higher at 3080 V.

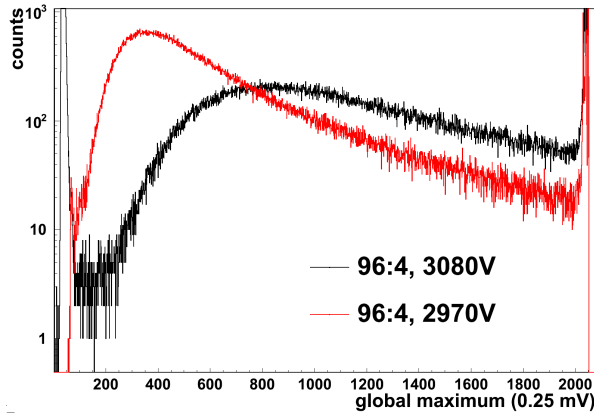


Figure 4.25: *Ar:CO₂ 96:4 at 3080 V and 2970 V - comparison of signal height spectra*

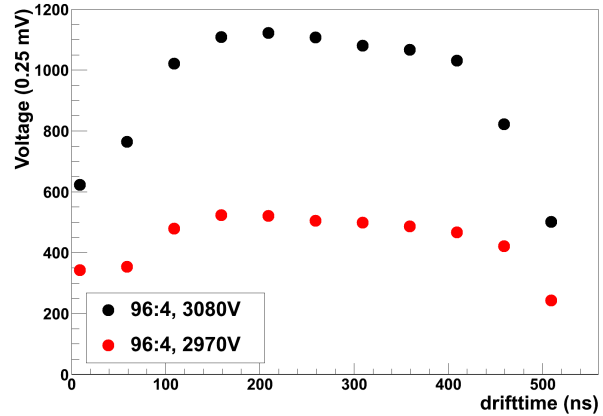


Figure 4.26: *Ar:CO₂ 96:4 at 3080 V and 2970 V - signal heights of averaged FADC signals. The averaged FADC signals are explained in 4.7.1*

In the end of signal spectra, figure 4.27, the shoulder is significantly reduced for 2970 V. This is due to the signal height dependence of the method for determining the signal end. For a further investigation of this effect, FADC signals will be studied in section 4.7.

Summarizing, in contrary to the drift time spectrum and the rt-relation, the changes in signal height and end of signal are significant, when operating at different anode voltages. The change in signal height was expected since in proportional mode an increase in voltage leads to greater gas amplification as treated in section 2.2.4. The small reduction in maximum drift time for reduced voltage can be explained with smaller elastic cross sections at higher electron energies, see figure 2.5.

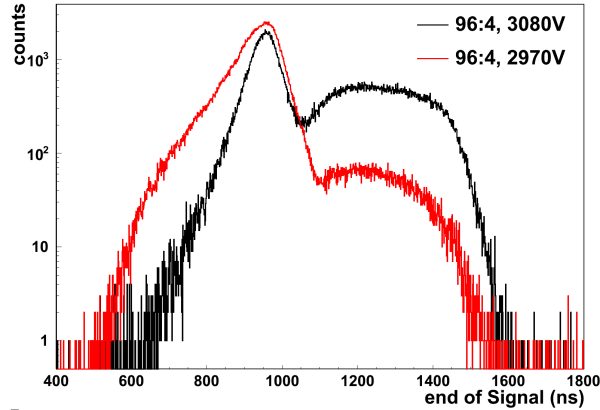


Figure 4.27: Ar:CO₂ 96:4 at 3080 V and 2970 V - comparison of end of signals

4.6 Results for Ar:CO₂:N₂ Gas Mixtures at Gas Gain 20 000

As seen earlier, the anode voltage has no large impact on drift time spectra and rt relations. For a better comparison of the signal end spectra, the gas mixture presented in this section were operated at gas gain 20 000, which is the same gas gain as at Ar:CO₂ 93:7 at 3080V.

In the following, the experimental results of gas mixtures which contain Ar and small CO₂ contents between 3 % and 4.5 % and additionally small N₂ amounts, will be presented. The presented gas mixtures are: Ar:CO₂:N₂ 95:4.5:0.5, 95:4:1, 96:3.5:0.5 and 96:3:1. All gas mixtures were operated at gas gain 20 000. As seen in section 4.4, the gas gain depends on the gas mixture. Therefore, the applied voltage for each gas mixture in order to obtain gas gain 20 000 differs from 3080 V. The required voltage for Ar:CO₂:N₂ 95:4.5:0.5 is 3030 V, for 95:4:1 it is 3035 V, for 96:3.5:0.5 it is 3004 V and 96:3:1 it is 3035 V.

The results can be seen in figures 4.28 to 4.31 and are compared to the standard gas mixture Ar:CO₂ 93:7. Figure 4.28 shows the measured **drift time spectra**. All tested gas mixtures have shorter drift time spectra in comparison to Ar:CO₂ 93:7, Ar:CO₂:N₂ 96:3:1 with $t_{max} = 438ns$ is the fastest one. The second fastest gas mixture is Ar:CO₂:N₂ 95:3.5:0.5 ($t_{max} = 453ns$) before 95:4:1 ($t_{max} = 482ns$) and 95:4.5:0.5 ($t_{max} = 509ns$). This suggests, that the maximum drift time scales with the CO₂ content. The drift time spectra of the tested gas mixtures show a shape which is more box like than the standard gas mixture.

Figure 4.29 shows the **rt-relations** of the tested gas mixtures. All gas mixtures are more linear and faster than Ar:CO₂ 93:7. The most linear gas mixture appears to be Ar:CO₂:N₂ 96:3:1.

All **signal height spectra** at gas gain 20 000, figure 4.30, are similar.

Figure 4.31 shows the **end of signal spectra**. For all gas mixtures the distribution maximum shifts to smaller times in comparison to the distribution maximum of the standard gas mixture. The gas mixture with the maximum at the smallest time is Ar:CO₂:N₂ 96:3:1, which is in accordance with its short drift time spectrum. For all tested gas mixtures the distributions are sharper but show a shoulder in comparison to the standard gas mixture. However, all signals end at the same point as Ar:CO₂ 93:7. This effect is not an electronic one, since for some gas mixtures the signal end spectra end after the spectrum for Ar:CO₂ 93:7, as will be seen later on (figure 4.38).

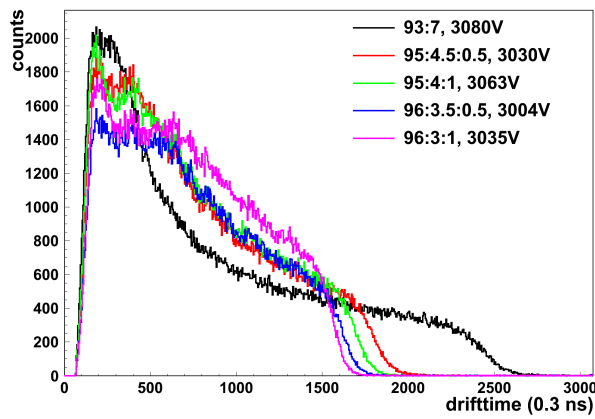


Figure 4.28: Ar:CO₂:N₂ gas mixtures - drift time spectra

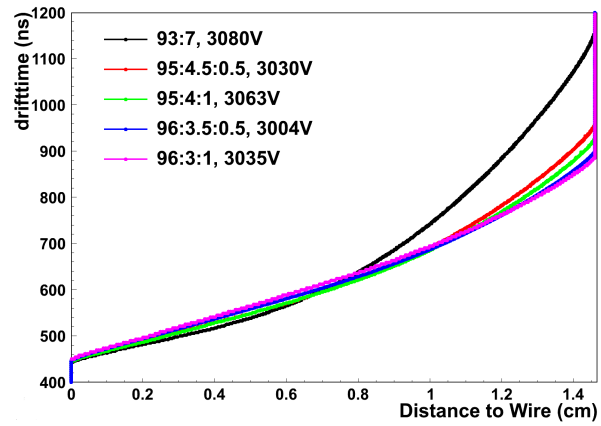


Figure 4.29: Ar:CO₂:N₂ gas mixtures - rt-relations

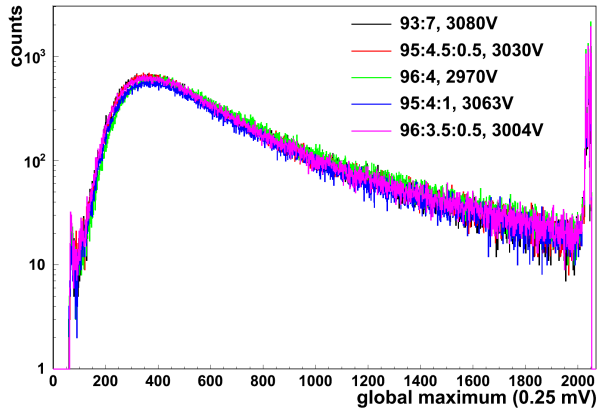


Figure 4.30: Ar:CO₂:N₂ gas mixtures - signal height spectra in logarithmic scale.

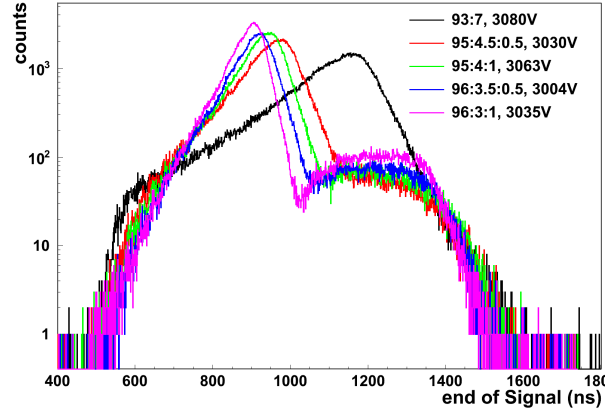


Figure 4.31: Ar:CO₂:N₂ gas mixtures - end of signal spectra. For Ar:CO₂:N₂ 96:3:1, 9.1 % of all events produce the shoulder in the end of signal spectra in logarithmic scale. This is not an electronic effect, see figure 4.38

4.7 Afterpulsing

This section treats the effect called *afterpulsing*. The afterpulsing refers to electrons reaching the wire after one maximum drift time, causing the shoulders in the end of signal determination. For all FADC spectra the offset - the time on the x-axis corresponding to $t_0 = 0ns$ - is fixed around 430 ns.

4.7.1 Averaged FADC Signals

To understand the shoulder in the signal end spectra for gas mixtures with small CO₂ contents, averaged FADC signals were studied. To obtain the averaged FADC signals, the FADC data of events with similar drift time intervals of $50 \pm 10ns$ are summarized and then divided by the number of events. Usually an averaged signal is averaged over several thousand single events. Averaged signals for the standard gas mixture Ar:CO₂ 93:7 are shown in figure 4.32. The following electronic effect is visible: signals with large integrated charge approach the baseline more slowly than signals with small integrated charge. Therefore, signals with short drift time last longer.

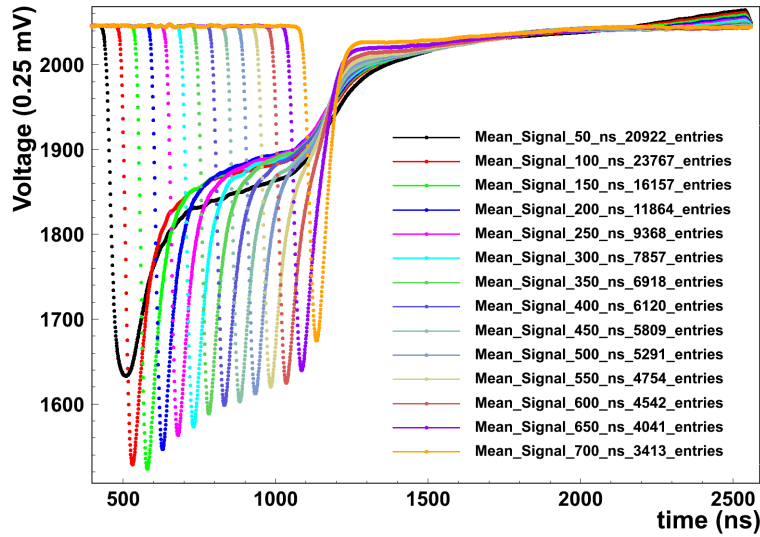


Figure 4.32: Averaged Signals for Ar:CO₂ 93:7, 3080 V, $t_{max} = 682ns + offset$

4.7.2 FADC Pulses after Maximum Drift Time

Figures 4.33 and 4.34 show averaged FADC signals for Ar:CO₂ 96:4 and Ar:CO₂ 97:3. These signals show pulses after the maximum drift time, in contradiction to the FADC signals of Ar:CO₂ 93:7, figure 4.32, where the signals drop fast after the maximum drift time. This means, that for the gas mixtures Ar:CO₂ 96:4 and Ar:CO₂ 97:3 a small amount of electrons is reaching the anode after the respective maximum drift time. More extended additional pulses are visible for the gas mixtures Ar:CO₂ 97:3, 3080 V, and Ar:CO₂:N₂ 96:2:2, 3141 V, figures 4.34 and 4.35. For Ar:CO₂:N₂ 97:2:1 at 3080 V even a third group of pulses is observed, figure 4.36.

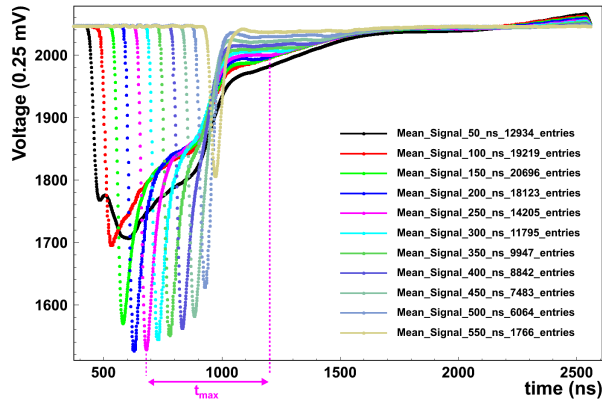


Figure 4.33: Averaged Signals for Ar:CO₂ 96:4, 2970 V, $t_{max} = 480ns + offset$. Additional pulses after t_{max} are observed.

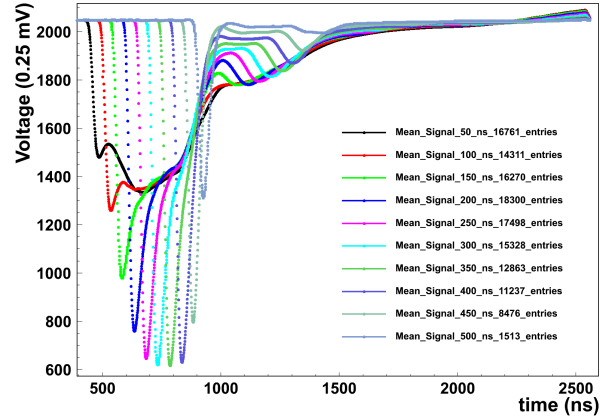


Figure 4.34: Averaged Signals for Ar:CO₂ 97:3, 3080 V, $t_{max} = 438ns + offset$. Additional pulses after t_{max} are observed.

Ar:CO₂:N₂ 97:2:1 at 3080 V is an example for large additional pulses. These pulses in figure 4.36 prove that the electronics is capable to record pulses beyond channel 1600. Therefore, the end of signal analysis in section 4.4 and 4.6 is sound. The signals of the analyzed Ar:CO₂ and Ar:CO₂:N₂ gas mixtures really end before channel 1600 as shown in the end of signal spectra, figure 4.31 and 4.22, and not being an artefact of electronics or data analysis. For the gas mixture Ar:CO₂:N₂ 97:2:1 at 3080 V with additional pulses the end of signal spectrum does not end around channel 1600 but extends to the maximum acquisition range of the FADC of 2500 ns, see figure 4.38.

These pulses after the maximum drift time are the reason for the shoulder in the end of the signal spectrum. Depending on the height of the pulse after the maximum drift time, the threshold used by the end of signal method crosses the signal already at this point and not around the maximum drift time. This effect is shown in figure 4.37.

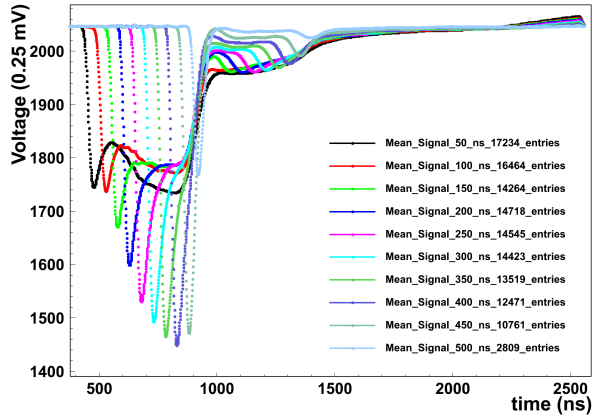


Figure 4.35: Averaged Signals for $\text{Ar}:\text{CO}_2:\text{N}_2$ 96:2:2, 3141 V, $t_{max} = 445\text{ns} + \text{offset}$. Additional pulses after t_{max} are observed.

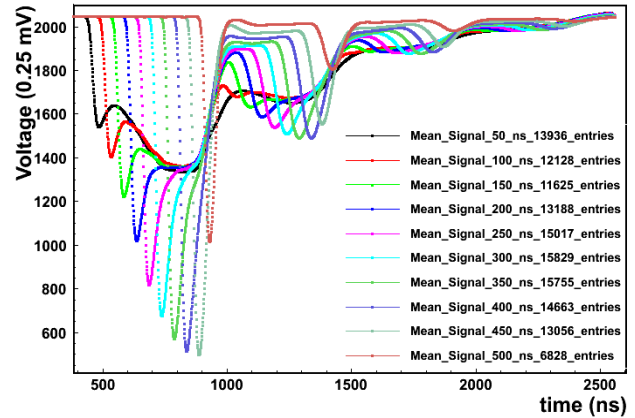


Figure 4.36: Averaged Signals for $\text{Ar}:\text{CO}_2:\text{N}_2$ 97:2:1, 3080 V, $t_{max} = 432\text{ns} + \text{offset}$. Second and even third group of pulses after t_{max} are observed.

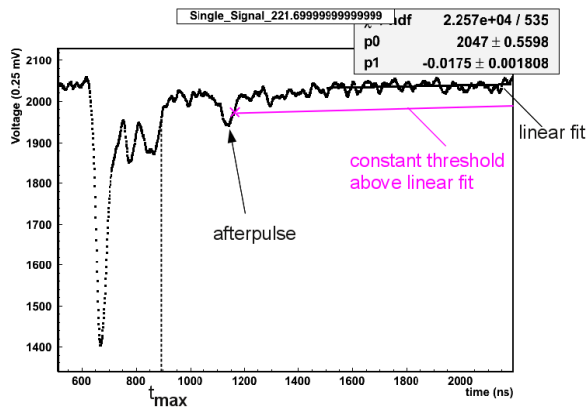


Figure 4.37: End of signal is misidentified at afterpulse, single event for $\text{Ar}:\text{CO}_2:\text{N}_2$ 96:2:2 3141 V

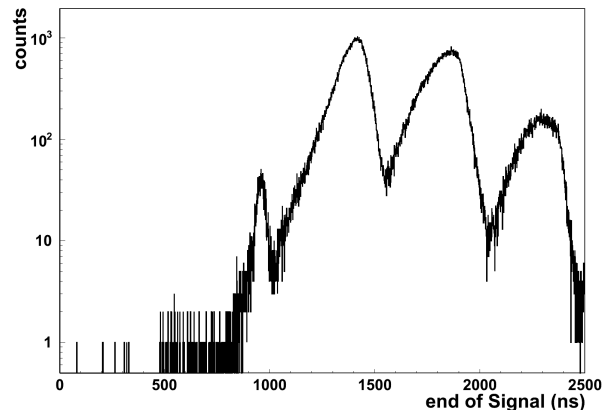


Figure 4.38: End of signal spectrum of $\text{Ar}:\text{CO}_2:\text{N}_2$ 97:2:1, 3080V

Time Difference between Pulses

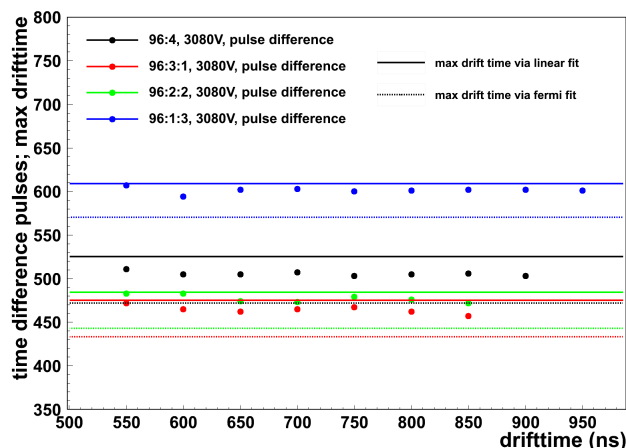


Figure 4.39: Time differences between first pulses and afterpulses in comparison to maximum drift times

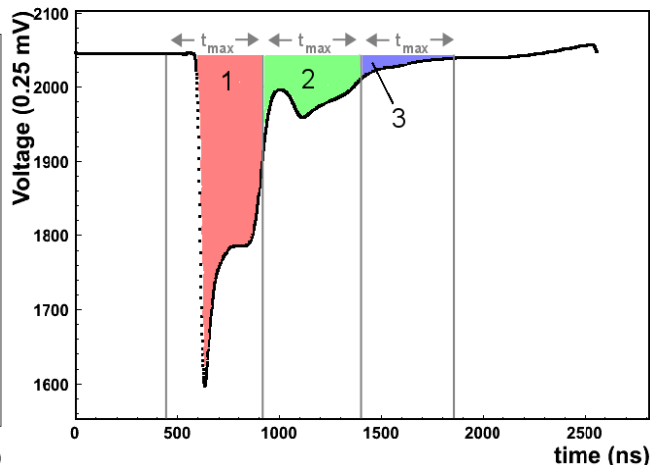


Figure 4.40: Integrals between signal and baseline at channel 2048 in intervals of t_{max} . The integrals are proportional to the number of electrons reaching the wire.

In order to understand the physics of the afterpulsing, the time difference between the first pulses and the pulses after the maximum drift time is investigated. It corresponds to approximately a maximum drift time, as illustrated in figure 4.33. In figure 4.39 the

- dots represent the time difference for each drift time
- dashed lines the maximum drift time determined by the *fermi fit method*
- solid lines the maximum drift time determined by the *linear fit method*

Figure 4.39 tells us that a clear correlation exists between the solid and the dashed lines and the points. The slower the gas mixture, the longer the time between the pulses. Furthermore, the time difference between the first pulse and the second pulse equals approximately one maximum drift time. However, the fermi and the linear fit method do not lead to the same results for the maximum drift times. When comparing the two methods one notices that the maximum drift times calculated by the fermi fit method have a constant offset below the points. In contrary, the linear fit method gives results that tend to be closer to the points, with varying deviation.

In conclusion: the time difference between the two FADC minima equals approximately one maximum drift time. The linear fit method gives maximum drift times close to the points, but their offsets are not as constant as the offsets of the fermi fit method.

Integrals of Second Pulses

In the following, the area between the FADC signals and the baseline at channel 2048 will be studied. As just seen, the pulses before and after the maximum drift time seem to be correlated by one maximum drift time. To study the integrals of the additional pulses, the just found correlation of one maximum drift time is used and the averaged signals are integrated in three intervals of one maximum drift time as shown in figure 4.40. In figure 4.41 these integrals can be seen for Ar:CO₂ 96:4 for different drift times. Figure 4.42 compares area 2 to area 1 and area 3 to area 2. Since the integral of the FADC signal is proportional to the number of electrons reaching the wire, this comparison should lead to an understanding about the correlation of the amount of electrons reaching the wire after the maximum drift time to the ones reaching it before the maximum drift time.

Figure 4.41 demonstrates, that the order of the first integrals coincides with the order of the second and third integrals. This means, that the more electrons are reaching the wire during the first maximum drift time, the more are reaching it during the second and third maximum drift time.

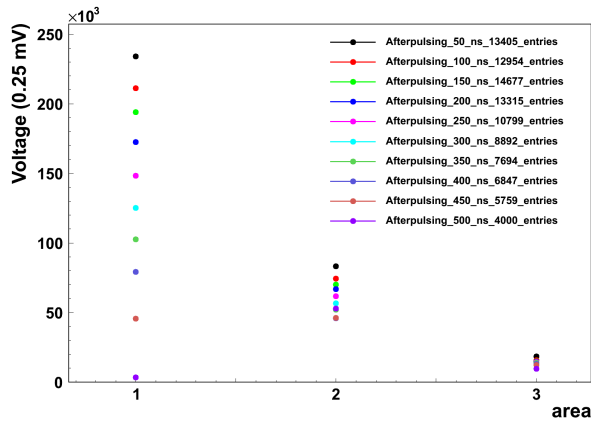


Figure 4.41: Integrals for Ar:CO₂ 96:4 averaged signals in terms of t_{max} as illustrated in figure 4.40, 3080 V. The different colours correspond to the respective drift time of the averaged signal.

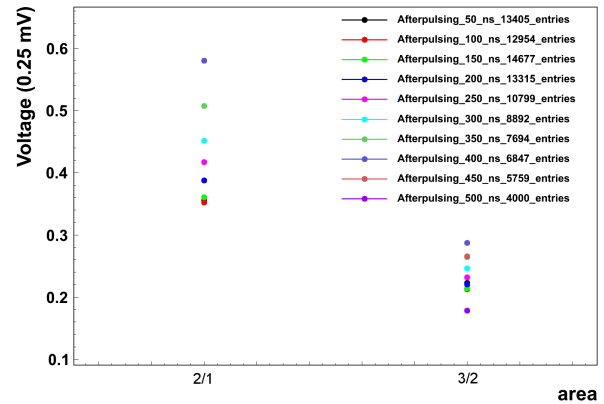


Figure 4.42: Ratios between Area 2 and 1 and between Area 3 and 2 for Ar:CO₂ 96:4, 3080 V

4.7.3 Physical Approach

A possible physical explanation for the observed afterpulsing considers photo effect at the tube wall, see figure 4.43. In the gas amplification region near the wire, the recombination of electrons and ions under emission of photons takes place. If the generated photons are in the appropriate energy range, they can then be absorbed by the tube wall under the emission of electrons. These electrons are created at the tube wall and thus need one maximum drift time for drifting towards the anode wire. In case of argon, the minimum energy of the emitted photons is 11.6 eV [25]. The ionization potential of the cathode material aluminum is 6.0 eV [22]. and is thus below the photon energy.

If a gas mixture contains next to argon also quencher gases which absorb photons, the afterpulsing is reduced. In order to understand the process of photon absorption inside a drift tube, the number of absorbed photons after traveling from the anode towards the tube wall is calculated in the following.

The ratio of absorbed photons can be calculated via

$$\frac{N}{N_0} = \exp(-n\sigma x) \quad (4.8)$$

where N is the number of photons before passing the gas, N_0 the number of the remaining photons after traveling distance x through a gas with gas density n and photoabsorption cross section σ . The photoabsorption cross section for argon and nitrogen at photon energies of 11.6 eV are around $0.3 \cdot 10^{-18} \text{cm}^{-2}$ and $0.25 \cdot 10^{-18} \text{cm}^{-2}$ [26], respectively, and for carbon dioxide around 10^{-17}cm^{-2} [27].

The gas density can be calculated by

$$n = \frac{N_A \cdot P}{V_{mo}} \quad (4.9)$$

where N_A denotes the Avogadro constant, p the pressure and V_{mo} the molar volume. The gas inside the tubes is at 3 bar pressure, thus the gas density equals $0.8 \cdot 10^{20} \frac{1}{\text{cm}^3}$. The photoabsorption by the argon atoms in gas mixture Ar:CO₂ 97:3 for photons traveling a distance of 1.5 cm (the tube radius) equals

$$\frac{N}{N_0} = \exp\left(-0.8 \cdot 10^{20} \frac{1}{\text{cm}^3} \cdot 0.97 \cdot 0.3 \cdot 10^{-18} \frac{1}{\text{cm}^2} \cdot 1.5 \text{cm}\right) = 2.699 \cdot 10^{-131} \quad (4.10)$$

This ratio would mean that nearly all photons are absorbed by the argon atoms. For carbon dioxide and nitrogen the number does not vary significantly since the photoabsorption cross sections are similar. This is not understood, since the for Ar:CO₂ 97:3 clear afterpulsing was observed as shown in figure 4.34.

The concept of afterpulses created due to photo effect at the tube wall is in accordance with the measurements: It was observed that the second pulses comes approximately one maximum drift time after the first pulses (figure 4.39). Assuming that the creation of

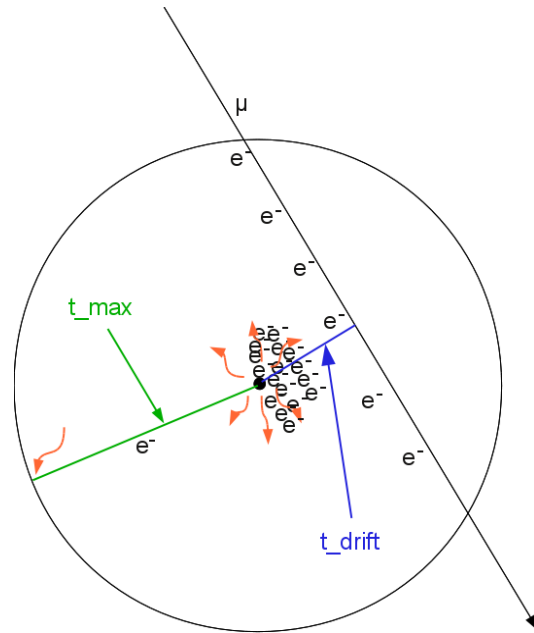


Figure 4.43: Photo effect at tube wall - possible explanation for second group of electrons

photons during the gas amplification process is correlated to gas amplification processes, the number of electrons created by the photoelectric effect should depend on the number of electrons reaching the wire during the first maximum drift time. This is observed when comparing the FADC integrals in intervals of maximum drift times (figure 4.41). The more electrons were registered during the first maximum drift time, the more electrons are registered during the second and third maximum drift time.

The observation of no additional pulses for Ar:CO₂ 93:7 (figure 4.32) in contrary to gas mixtures with less amount of quencher gas contents (figure 4.33 - 4.36) where additional pulses are observed, is in accordance with the assumption that quencher gases absorb photons leading to less afterpulsing.

The afterpulsing should be avoided because it enlarges the occupancy and could lead to new triggers and more incoming electrons increase ageing effects.

4.7.4 Afterpulse Amplitudes and Integrated Afterpulse Spectra

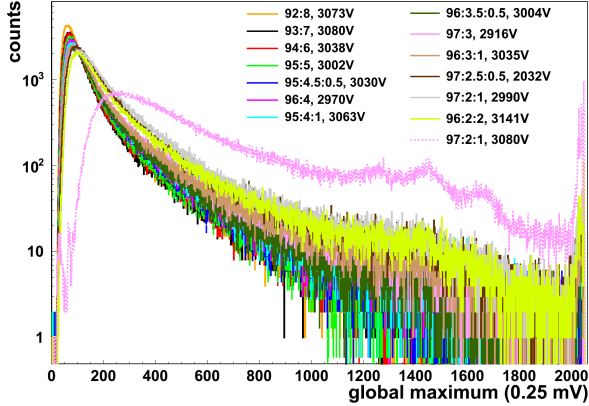


Figure 4.44: Afterpulse amplitude spectra: signal heights after $t_{max} + 10ns$. All gas mixtures are at measured gas gain 20 000 except for Ar:CO₂ 97:3 at 30808 V.

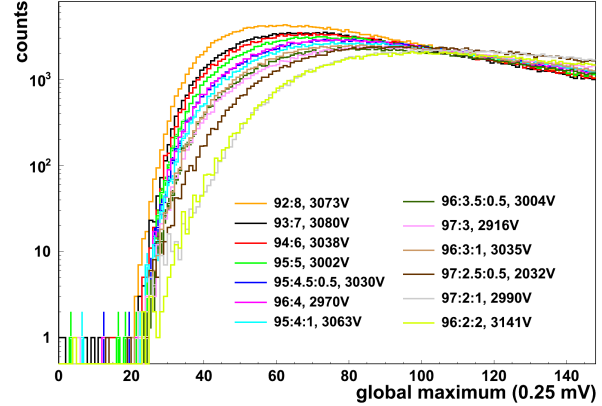


Figure 4.45: Afterpulse amplitude spectra: signal heights after $t_{max} + 10ns$. All gas mixtures are at measured gas gain 20 000. Zoomed view.

So far, averaged signals were used to characterize the shape of the FADC signals. However, they don't give much information about fluctuations of single signals around the averaged signal. Therefore, in order to study the single signal fluctuations of the afterpulsing, amplitude spectra after one maximum drift time were created. This was done by determining the global minimum between $t_{max} + 10ns$ and the end for every signal.

Furthermore, spectra of integrated pulses from $t_{max} + 10ns$ and the signal end were created in order to study the amount of electrons reaching the wire after one maximum drift time. The results will be examined in the following.

The afterpulse amplitude spectra are shown in figure 4.44 and 4.45 and the integrated afterpulse spectra in figure 4.46 and 4.47. For the afterpulse amplitude spectra in figure 4.44, the distribution maximum is at a clearly higher voltage for gas mixture Ar:CO₂ 97:3 at 3080 V (gas gain around 60 000). This gas mixture has shown a strong afterpulsing in the averaged signals. The maxima of gas mixtures with gas gain 20 000 range from around $70 \cdot 0.25$ mV for Ar:CO₂ 93:7 without afterpulsing to $110 \cdot 0.25$ mV for Ar:CO₂:N₂ 97:2:1 with a small observed afterpulsing in the averaged signals and are therefore more or less in the same region, see in figure 4.45.

The maxima of the integrated afterpulse spectra for gas mixtures at gas gain 20 000 range from 20 000 for Ar:CO₂ 93:7 to 30 000 for Ar:CO₂:N₂ 97:2:1. This means that for a gas mixture with a small observed afterpulsing in the averaged pulses, most likely 0.5 times more electrons reach the wire after a maximum drift time than for the standard gas mixture. However, both fast and linear gas mixtures, Ar:CO₂ 97:3, Ar:CO₂:N₂ 96:3.5:0.5

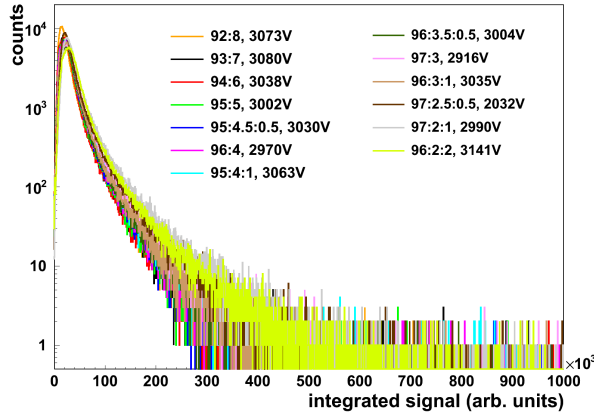


Figure 4.46: Integrated afterpulse spectra: integrated signals after maximum drift time. All gas mixtures are at measured gas gain 20 000. The total integral of Ar:CO₂ 93:7 from t_0 to t_{max} peaks average at channel 85000

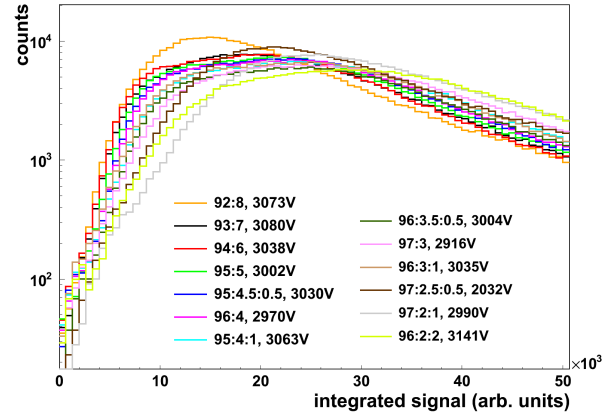


Figure 4.47: Integrated afterpulse spectra: integrated signals after maximum drift time. All gas mixtures are at measured gas gain 20 000. The integral of Ar:CO₂ 93:7 from t_0 to t_{max} is in average at 85000. Zoomed view.

and 96:3:1, do not show strong increase in electron arrival, as seen in figure 4.48.

4.7.5 Streamer Signals

Streamer pulses are expected to occur for Ar:CO₂ with a probability below 0.1%. These pulses create about a factor of 100 more charges than standard proportional pulses and should show up beyond channel 10^6 in figure 4.46. For the promising gases Ar:CO₂:N₂ 96:3:1, 96:3.5:0.5, 97:2.5:0.5 and Ar:CO₂ 97:3 no streamer signals were observed for data samples of 300 000 events.

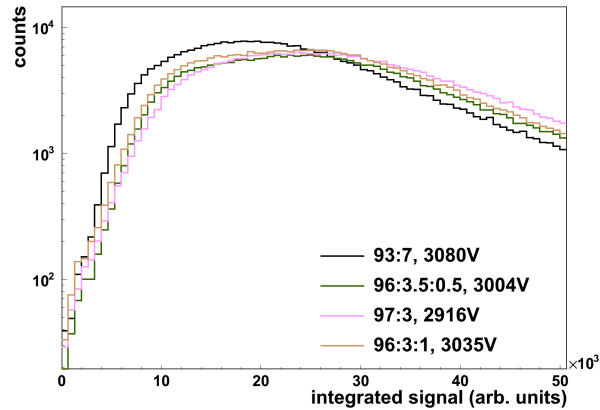


Figure 4.48: Integrated afterpulse spectra: integrated signals after maximum drift time for promising gas mixtures.

4.7.6 Single Events

This section discusses and compares signals for single events for the standard gas mixture Ar:CO₂ 93:7 at 3080 V, for a gas mixture with large afterpulsing Ar:CO₂:N₂ 97:2:1 at 3080 V and the fast gas mixture with small afterpulsing Ar:CO₂:N₂ 96:3:1 at 3035 V.

Ar:CO₂ 93:7, 3080 V:

Figure 4.49 and 4.50 show two single events for the standard gas mixture Ar:CO₂ 93:7. The signals drop down after the maximum drift time exponentially, it takes until 1700 ns to reach the base line (offset 430 ns).

Ar:CO₂:N₂ 97:2:1, 3080 V:

Two single events for gas mixture Ar:CO₂:N₂ 97:2:1 at 3080 V are shown in figures 4.51 and 4.52. These signals show afterpulses. Here, each sub peak of the signal is repeated three times. It hence needs a long time to drop down.

96:3:1 at 3035 V:

There are two single events for gas mixture 96:3:1 at 3035 V shown in figure 4.53 and 4.54. The signals decrease like pulses in Ar:CO₂ 93:7 after the maximum drift time and don't show considerable afterpulses.

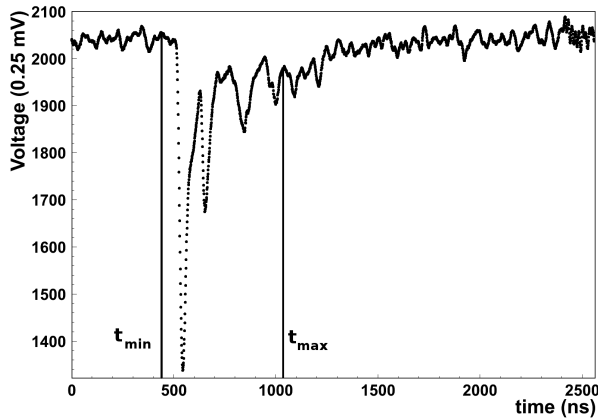


Figure 4.49: Single Event Ar:CO₂ 93:7, 3080 V, $t_{drift} = 111$ ns

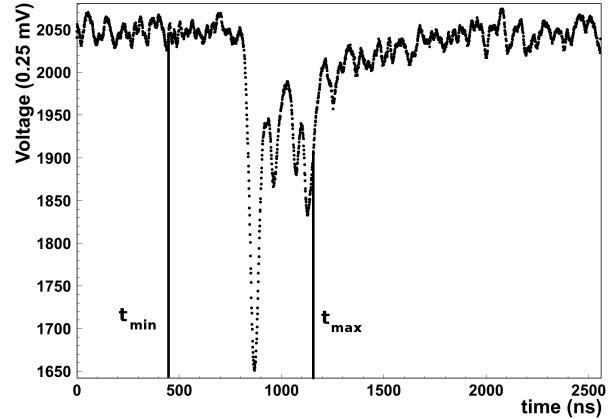


Figure 4.50: Single Event Ar:CO₂ 93:7, 3080 V, $t_{drift} = 420$ ns

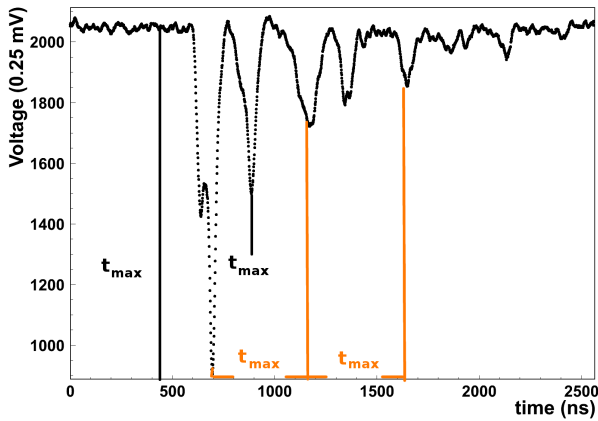


Figure 4.51: Single Event Ar:CO₂:N₂ 97:2:1, 3080V, $t_{drift} = 199$ ns

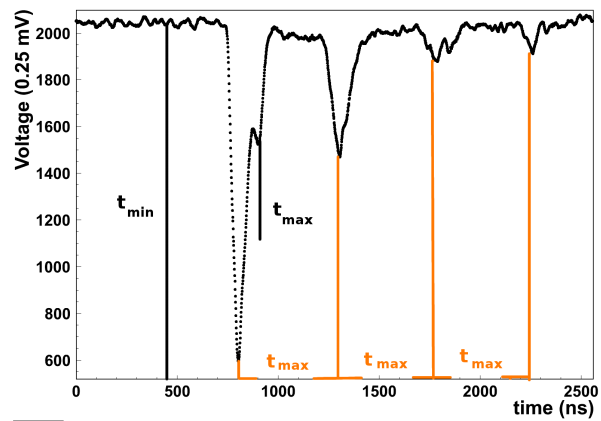


Figure 4.52: Single Event Ar:CO₂:N₂ 97:2:1, 3080V, $t_{drift} = 342$ ns

4.8 Summarized Experimental Results

This section summarizes the experimental results of maximum drift time, linearity, gas amplification, afterpulsing and streamer probabilities for all measured gas mixtures and compares them to the simulation. Tables 4.1 and 4.2 list all tested gas mixtures at 3080 V and at gas gain 20 000, respectively. Since a gas gain of 20 000 is preferable, the results of all gas mixtures with gas gain 20 000 will be presented in the following. Additionally, the gas mixture Ar:CO₂:N₂ 96:1:3 at 3080 V will be included, since this gas mixture has not been measured at gas gain 20 000 due to the high required voltage. However, as seen in section 4.5, the results in maximum drift time and linearity should not differ significantly at different gas gains.

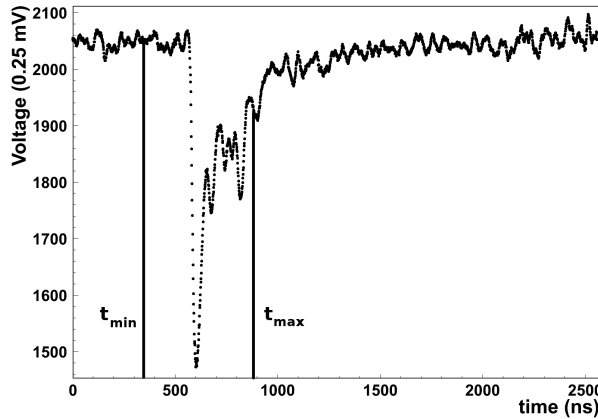


Figure 4.53: Single Event
Ar:CO₂:N₂ 96:3:1, 3035V,
 $t_{drift} = 170$ ns

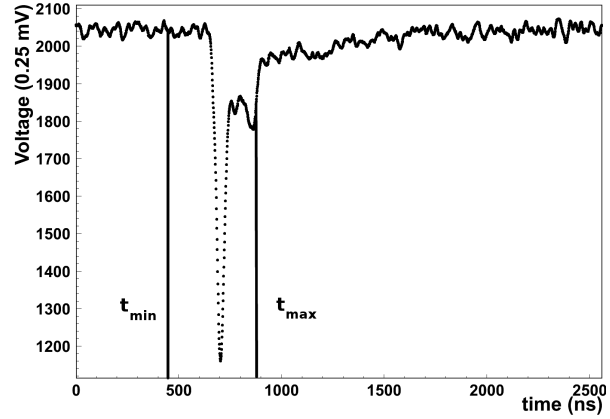


Figure 4.54: Single Event
Ar:CO₂:N₂ 96:3:1, 3035V,
 $t_{drift} = 320$ ns

All results are plotted against the CO₂ content on the x-axis with the N₂ content encoded in colours. The Ar content sums up to 100%. For example, the green (2% N₂) dot at 2% CO₂ in figure 4.55, refers to the measured maximum drift time for gas mixture 96:2:2.

Ar (%)	CO ₂ (%)	N ₂ (%)	voltage (V)	voltage for gas gain 20 000 (V)
82	8	9	3080	3073
93	7	0	3080	3080
94	6	0	3080	3038
95	5	0	3080	3002
96	4	0	3080	2970
97	3	0	3080	2916
96	3	1	3080	3035
96	2	2	3080	3141
93	2	5	3080	-
96	1	3	3080	-

Table 4.1: Measured gas mixtures at 3080 V and anode voltage corresponding to gas gain 20 000. The two three gas mixtures were measured at gas gain below 20 000 only.

Ar (%)	CO ₂ (%)	N ₂ (%)	voltage (V)	t_{max} (ns)	χ^2_{ndf}	afterpulse (%)	t_{quiet} (ns)	signal height > 2020 ch. (%)	amplitude _a > 90 channels (%)	integrated _a > 19980 (%)
92	8	0	3073	800	3989.98	0.227749	802	0.0275401	0.528196	0.41
93	7	0	3080	712	2966.29	0.244922	725	0.0345699	0.561567	0.552228
94	6	0	3038	627	2095.09	0.275481	652	0.0326716	0.586437	0.57011
95	5	0	3002	551	1299.62	0.302109	585	0.036913	0.62824	0.62
95	4.5	0.5	3030	509	911	0.322916	549	0.038824	0.675859	0.665795
96	4	0	2970	491	621.465	0.333193	529	0.0390292	0.671331	0.668386
95	4	1	3063	482	634.886	0.328944	521	0.0465574	0.706576	0.71
96	3.5	0.5	3004	453	378.978	0.357374	498	0.0428902	0.730567	0.719406
97	3	0	2916	445	153.243	0.408586	496	0.0394584	0.767506	0.766411
96	3	1	3035	438	214.004	0.363381	480	0.0418848	0.737845	0.72
97	2.5	0.5	2932	425	69.4069	0.426583	478	0.0436496	0.840575	0.73
97	2	1	2990	436	26.0353	0.465499	497	0.044422	0.885537	0.84
96	2	2	3141	449	38.7906	0.441393	505	0.0467171	0.85972	0.837376
93	2	5	3250	485	47.6087	0.369084	483	(0.00121227)	(0.274906)	(0.213955)
96	1	3	3080	570	358.394	0.456817	570	(0.000845327)	(0.265606)	(0.283072)

Table 4.2: Experimental results of gas mixtures gas gain 20 000. Desirable properties are given in green, acceptable ones in orange and poor ones in blue. Gas mixture Ar:CO₂:N₂ 93:2:5 was measured at 3250 V with gas gain around 7000, gas mixture Ar:CO₂:N₂ 96:1:3 at 3080 V with gas gain around 8500. Thus the values for these gas mixtures are given in brackets.

The maximum drift time t_{max} was obtained from the drift time spectra to which fermi fits were performed, as described in section 4.3.1 and illustrated in figure 4.9. In order to determine the linearity, the same method as for the simulated rt -relations, as described in section 3.2, was applied: A linear function was fitted to the measured rt -relations giving $\frac{\chi^2}{ndf}$. The voltage was chosen in order to obtain gas gain 20 000. The afterpulse is given in terms of electrons reaching the wire during the interval one maximum drift time after the first maximum drift time (area 2 in comparison to area 1 as in figure 4.40). t_{quiet} corresponds to the time after which the amplitude in more than 70% of the events is only small (\cong signal does not cross end of signal line as in figure 4.6). The "large signal" column refers to the percentage of signals with signal heights larger than 2020 channels in order to look for indications of streamer signals. The last two columns give the percentage of events with afterpulse amplitudes larger than 90 channels and integrated afterpulses larger than 18000. Streamer signals would also appear in the number integrated afterpulses larger than 18000, since in streamer mode a large amount of charge is collected.

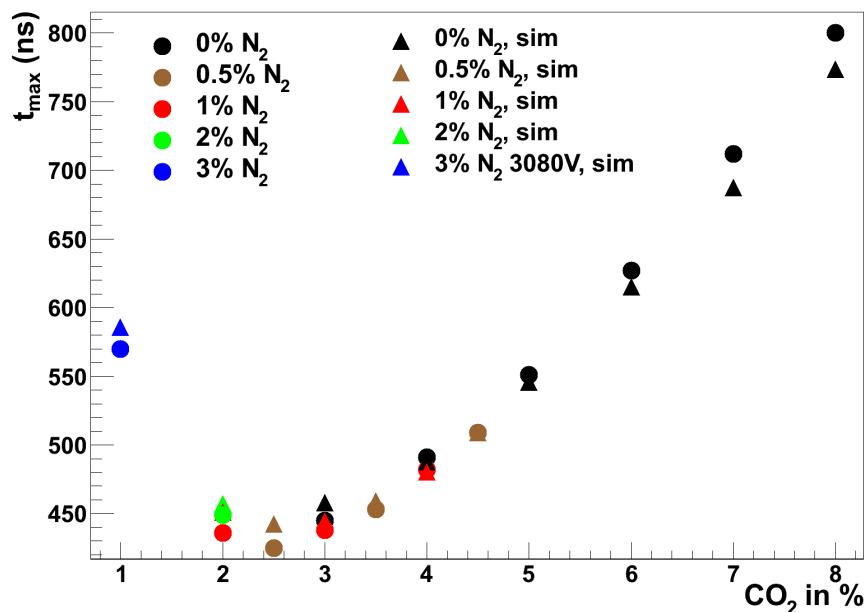


Figure 4.55: Maximum drift time of measured gas mixtures (dots) and simulation (triangles). The maximum drift time shows a minimum for 2.5% CO₂. The simulated values for Ar:CO₂:N₂ 97:2:1 is hidden behind the measured data point for Ar:CO₂:N₂ 96:2:2. For CO₂ values between 3.5% and 4.5% the simulations are in very good agreement and therefore the measured and simulated points overlap.

4.8.1 Maximum Drift Time

The dots in figure 4.55 represent measured maximum drift times obtained from the drift time spectra by the fermi fit method. The triangles show the simulated results. The measured maximum drift times (dots) show a curve which is mainly influenced by the CO₂ content. The N₂ addition of 1% shows a small, but positive impact, decreasing the maximum drift time by 7 ns and 13 ns for gas mixtures containing 3% and 4 % CO₂, respectively. For 2% CO₂ the addition of 2% N₂ has a negative effect, increasing the maximum drift time by 13 ns.

The fastest gas mixtures contain between 2% and 4% CO₂ with a minimum at 3% CO₂. The gas mixture with the shortest maximum drift time is Ar:CO₂:N₂ 96:3:1 with $t_{max} = 438$ ns which is 38% faster than the standard gas mixture Ar:CO₂ 93:7 with $t_{max} = 712$ ns.

The measured gas mixtures indicate the same trends concerning the CO₂ and N₂ content compared to the simulations. The measured maximum drift times exceed the simulated values by only 5% or better.

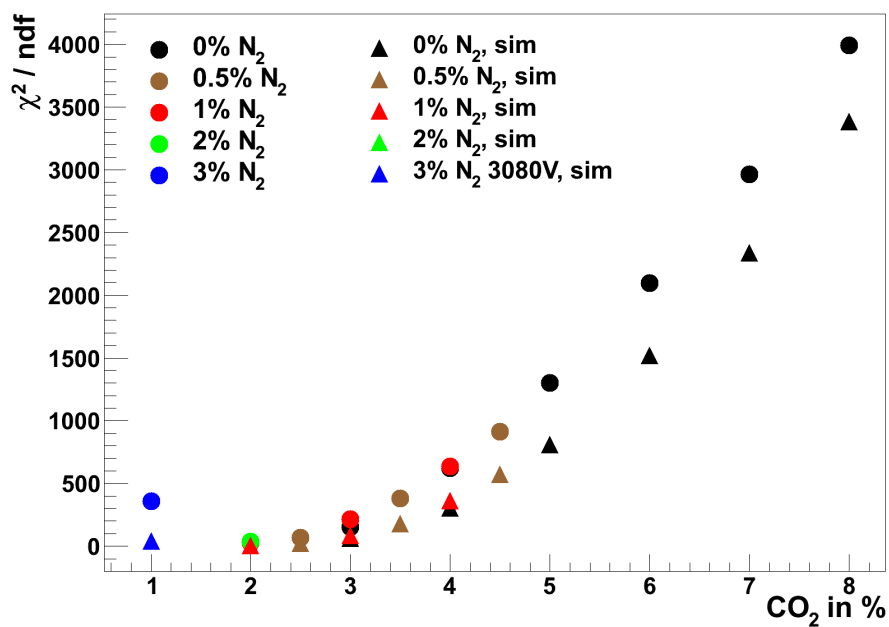


Figure 4.56: Linearity: ratio between likelihood ratio χ^2 and the number of degrees of freedom (ndf) for measured gas mixtures (dots) and simulation (triangles). Most linear gas mixtures contain between 1% and 4% CO₂ with a minimum at 2% CO₂. The measured data point for Ar:CO₂:N₂ 97:2:1 is hidden behind measured data point for Ar:CO₂:N₂ 92:2:2. The simulated data point for Ar:CO₂:N₂ 92:2:2 is hidden behind simulated data point for Ar:CO₂:N₂ 97:2:1.

4.8.2 Linearity

The linearity of the measured rt-relations is determined in the same way as for the simulated ones which is described in section 3.2. The dots in figure 4.56 represent the χ^2 divided by the number of degrees of freedom of a linear fit function to the measured rt-relations.

The curve is dominated by the CO₂ content. In the experimentally studied region, N₂ indicates a very small, but negative influence on linearity regarding gas mixtures with same CO₂ content but different N₂ content. The most linear gas mixtures contain between 1% and 3% CO₂ with a minimum of $\frac{\chi^2}{ndf}$ at 2% CO₂. The most linear measured gas mixtures are Ar:CO₂:N₂ 97:2:1 and 96:2:2. Ar:CO₂ 98:2 was not experimentally studied due to potential high voltage breakthrough.

In comparison to the simulations, the simulated gas mixtures are up to 25% more linear than the measured gas mixtures. Still, the simulations show the same trends as the measurement with best linear gas mixtures at 2% CO₂.

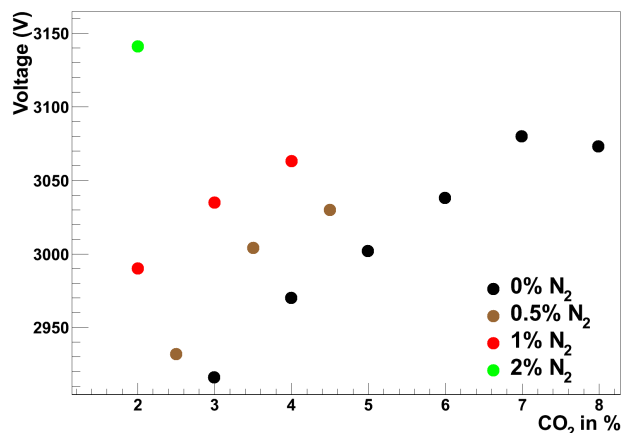


Figure 4.57: Required voltage for gas gain 20 000. Addition of N₂ leads to higher voltage. The gas gain increases with temperature. Since some gas mixtures were measured during winter and some during summer time, temperature variation is not negligible. During winter time the following gas mixtures were measured: Ar:CO₂:N₂ 93:7:0, 94:6:0, 95:5:5, 96:4:0, 96:3.5:0.5, 95:4.5:0.5, 96:3:1, 95:4:1, 96:2:2. During summer time the following gas mixtures: Ar:CO₂:N₂ 92:8:0, 97:3:0, 97:2.5:0.5, 97:2:1

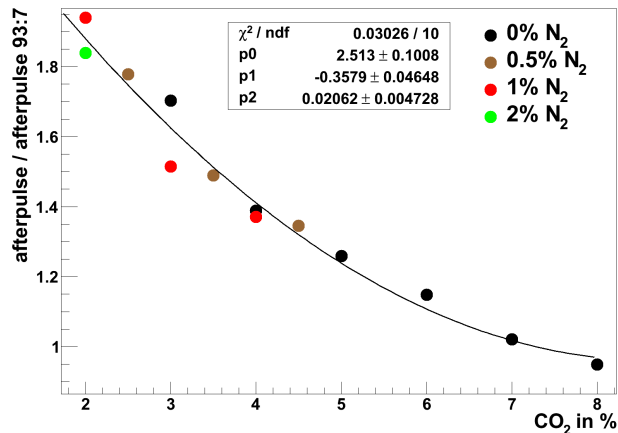


Figure 4.58: Afterpulsing: Normalized ratios between areas 2 and 1 as described in figure 4.40. Afterpulsing increases with less CO₂ and N₂ fractions. Nitrogen seems to absorb less photons than carbon dioxide.

4.8.3 Voltage for Gas Gain 20 000

To avoid ageing, gas gain of 20 000 is preferable, therefore the required voltages for an operation at gas gain 20 000 for the measured gas mixtures are studied. The results are shown in figure 4.57. The voltage depends heavily on both, the CO₂ and the N₂ content. In general, the voltage is smaller the less CO₂ and N₂ the gas mixture contains, allowing to reduce the voltage from 3080 V for Ar:CO₂ 93:7 to 2916 V for Ar:CO₂ 97:3. N₂ has a stronger impact on the gas gain than CO₂ since for example the required voltage for Ar:CO₂:N₂ 96:3:1 at 3035 V is 45 V larger than for Ar:CO₂ 96:4. For the gas mixture Ar:CO₂:N₂ 92:2:2 a voltage of 3141 V has to applied, which supports the assumption that the addition of N₂ leads to a considerable decrease in gas gain. The gas mixtures were not measured at constant temperature, but some were measured during winter time and some during summer. The gas gain depends on the temperature as studied in [14]. The exact temperature was not logged for the measurements, but the caption of figure 4.57 denotes the season the measurements took place.

4.8.4 Afterpulsing

In figure 4.58 the ratios between integrals after the maximum drift time and integrals before the maximum drift time, averaged over all drift times and normalized to Ar:CO₂ 93:7, are plotted. The integrals are illustrated in figure 4.40. All gas mixtures were operated at gas gain 20 000.

The curve is dominated by the CO₂ content. Less CO₂ contents lead to more afterpulsing. However, at low CO₂ values, a N₂ content between 1% and 2% seems to reduce the afterpulsing, see data points 2% and 3% CO₂ for different N₂ values in figure 4.58.

The comparison of gas mixtures with equal Ar content but different ratios of N₂ and CO₂ let conclude on the photoabsorption of N₂ and CO₂. The measurements let conclude, that nitrogen absorbs less photons than carbon dioxide, since the data points are higher for fewer CO₂ and larger N₂ contents. As example, the afterpulsing of Ar:CO₂ 96:4 is smaller than for Ar:CO₂:N₂ 96:3:1.

4.8.5 Afterpulse Amplitude Spectra and Integrated Afterpulse Spectra

Figure 4.59 shows the number of events with afterpulse amplitudes larger than 90 channels in percentage of all recorded events. The numbers were extracted from the amplitude spectra 4.44 and are at 52.2% for Ar:CO₂ 92:8 and increase with falling CO₂ content to 88.5% for Ar:CO₂:N₂ 97:2:1.

Figure 4.60 shows the number of events with afterpulse integrals larger than 19980. The values result from the integrated afterpulse spectra 4.46.

The data points follow the same trend as the previous study of the afterpulse signal height spectra. For the standard gas mixture Ar:CO₂ 93:7 the percentage of events with large afterpulse integrals is 55.2%. The number increases up to 84.9% for gas mixture Ar:CO₂:N₂ 97:2:1, see figure 4.60.

In conclusion, even for the standard gas mixture Ar:CO₂ 93:7, which shows a small afterpulsing, 56.2% of the events have still large signals after $t_{max} + 10ns$. For the linear and fast gas mixture Ar:CO₂:N₂ 96:3:1 this number lies at 73.8% for high afterpulse amplitudes and at 0.72% for large afterpulse integrals.

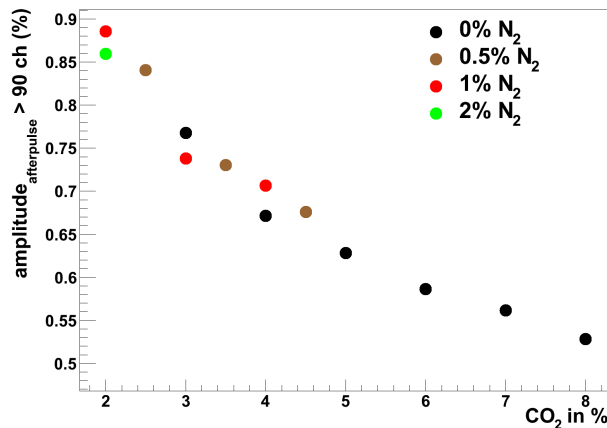


Figure 4.59: Afterpulse amplitudes larger than 90 channels (22.5 mV)

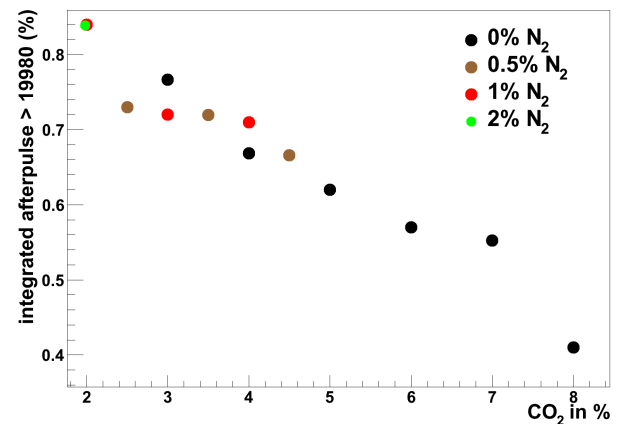


Figure 4.60: Afterpulse integrals larger than 19980. Data point for Ar:CO₂:N₂ 97:2:1 is hidden behind Ar:CO₂:N₂ 96:2:2.

4.8.6 Time after which Signals have Dropped Down

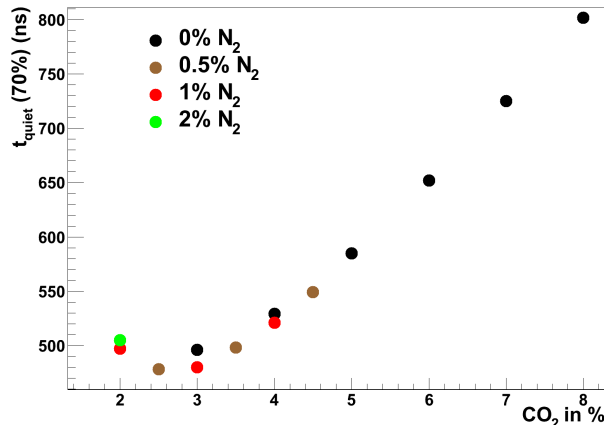


Figure 4.61: Time after which 70% of signals have dropped down.

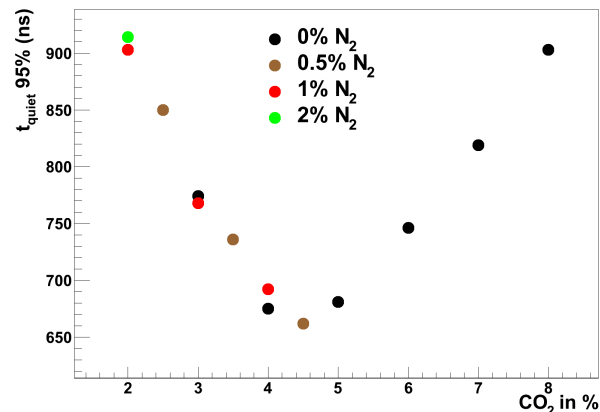


Figure 4.62: Time after which 95% of signals have dropped down.

Figure 4.61 shows the times after which the signals in 70% of the events have reached the base line. This time was obtained by the end of signal method illustrated in figure 4.6. The analysis shows, that despite the afterpulsing of mixtures with low CO₂ content, the faster gas mixtures still end earlier in 70% of the events than slower gas mixtures without afterpulsing like Ar:CO₂ 93:7.

Figure 4.62 shows the times after which the signals in 95% of the events have dropped down. It is observed, that this time increases for gas mixtures with smaller CO₂ contents and increases afterpulsing. However, between for gas mixtures with 3% to 6% CO₂ the signals drop down faster than the standard gas mixture.

In conclusion, fast gas mixtures reduce the time the signals take to drop down by 12% in 70% of the events and by 20% in 95% of the events.

4.8.7 Streamer Properties

Large signals might indicate that the detector operates in streamer mode. Streamer mode means that gas amplification is increased in a way that the number of electrons reaching the wire is no longer proportional to the number of primary electrons, as described in section 2.2.4.

Figure 4.63 shows the number of signals with signal height larger than 2020 channels divided by the total number of measured events at gas gain 20 000. The number of events with large signals increases for smaller CO₂ contents ranging from 3.7% to 5.4% of the recorded events.

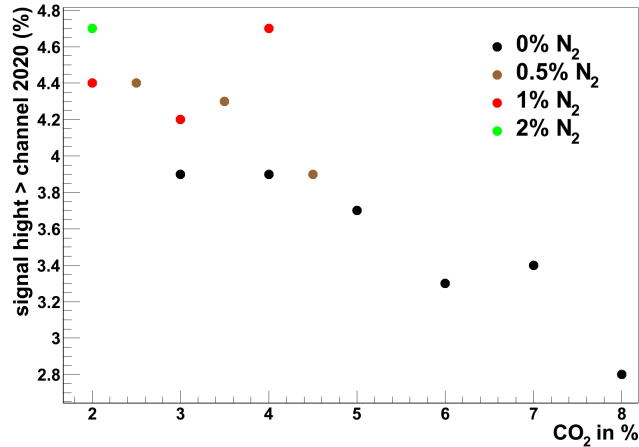


Figure 4.63: Signals with signal height larger than 2020 channels

Additionally, the analysis of figure 4.46 shows no indication for streamer signals at the gas mixtures Ar:CO₂:N₂ 96:3:1, 96:3.5:0.5, 97:2.5:0.5 and Ar:CO₂ 97:3.

4.8.8 Summary

With respect to the previous section, the experimental result lead to a few candidate gas mixtures which are in the appropriate range for all drift gas criteria. These gas mixture are Ar:CO₂ 97:3, Ar:CO₂:N₂ 97:2.5:0.5, 96:3.5:0.5 and 96:3:1. Ar:CO₂:N₂ 97:2.5:0.5 is the fastest and most linear gas mixture, however it shows larger afterpulsing. Ar:CO₂:N₂ 96:3.5:0.5 and 96:3:1 and Ar:CO₂ 97:3 are quite similar, but Ar:CO₂:N₂ 96:3:1 shows slightly better properties in all categories.

In [15] measurements without irradiation show that gas mixtures Ar:CO₂:N₂ 96:3:1 and 97:2:1 have a similar resolution to Ar:CO₂ 93:7. Since these gas mixtures are more linear, the resolutions are expected to deteriorate less under irradiation than for Ar:CO₂ 93:7. This could be proven recently by A. Engl [16]. At gamma rates of 19 000 Hz/cm² the resolution deteriorates considerably less at the use of the drift gas Ar:CO₂:N₂ 96:3:1.

Chapter 5

Conclusions

Higher luminosities at LHC lead to more irradiation background for the MDT chambers at the ATLAS detector, and therefore to deterioration of the spatial resolution. In order to avoid the resolution deterioration, the chambers could be replaced by new hardware. Since this is accompanied by high costs and effect. Thus, this thesis focuses on the search for a new drift gas with less resolution deterioration under high rate irradiation. The standard gas mixture used currently at ATLAS, Ar:CO₂ 93:7, is slow and non-linear. Within this thesis, Ar:CO₂ and Ar:CO₂:N₂ gas mixtures were examined by simulations and measurements with respect to maximum drift time, linearity, afterpulsing, gas gain and streamer probability.

In chapter 1, the selection procedure for the standard mixture Ar:CO₂ 93:7 is explained. Chapter 2 treats next to the working principle of the MDT chambers also their physical background and the requirements for an optimized drift gas.

Chapter 3 presents simulation results. The electron drift velocity, maximum drift time and linearity are simulated for various ratios of Ar:CO₂ and Ar:CO₂:N₂. Finally the influence of the applied anode voltage is studied.

The simulated drift velocity of Ar:CO₂ 93:7 depends strongly on the electric field and is small for small electric fields and large for large fields. The reduction of the CO₂ content increases the velocity at smaller fields and decreases it at higher fields, making it thus more constant and less dependent on the electric field. The addition of N₂ shows no extensive effect at small fields, but increases the velocity at high fields around 10⁴ V/cm.

As results on the linearity, the optimum CO₂ amount is found between 1% and 4%. Further improvement in linearity can be achieved for gas mixtures with CO₂ of 1% or 2% contents by adding of small amounts of N₂ up to 1.4%.

Concerning the maximum drift time, fast mixtures contain between 2% and 4% CO₂. The addition of small N₂ contents up to 1.2% shows a positive influence reducing the maximum drift time.

The drift velocity comparison of gas mixtures at 3080 V and at voltages with gas gain around 20000 gives no significant differences.

In chapter 4, experimental results are given after the description of the experimental set up the data analysis.

The analysis of the FADC signals showed that with reduction of CO_2 , additional pulses after one maximum drift time occur. A physical explanation for this effect is that photons, that are created due to recombination of electrons and ions during the gas amplification process, lead to photo effect at the tube wall and create new electrons, which then drift towards the wire. Studying the pulse maxima shows that the time difference between them equals one maximum drift time which is in accordance with the assumption.

The $\text{Ar}:\text{CO}_2$ and $\text{Ar}:\text{CO}_2:\text{N}_2$ measurements were analyzed with respect to the maximum drift time, the linearity, the required voltage for gas gain 20000. Furthermore, the gas mixtures were analyzed concerning the time after which the gas mixture is quiet, concerning the afterpulsing and the streamer probabilities. The experimental results on maximum drift time and linearity are in accordance with the simulations. The fastest gas mixture, $\text{Ar}:\text{CO}_2:\text{N}_2$ 97:2.5:0.5, is 38% faster than the standard mixture. Fast mixtures contain between 2% and 4% CO_2 . Linear gas mixtures contain between 1% and 4% CO_2 . The addition of N_2 in the studied range between 0.5% and 5% shows a small but slightly negative effect on linearity. Small afterpulsing has been observed in the FADC signals. However, the signals of fast gas mixture with afterpulsing still end earlier than slow mixtures without afterpulsing.

Good candidates for an alternative drift gas are $\text{Ar}:\text{CO}_2:\text{N}_2$ 97:2.5:0.5, $\text{Ar}:\text{CO}_2:\text{N}_2$ 96:3.5:0.5, $\text{Ar}:\text{CO}_2:\text{N}_2$ 96:3:1 and $\text{Ar}:\text{CO}_2$ 97:3. The experimental and simulation results on these gas mixtures are in good agreement.

The candidates still have to be investigated with respect to ageing effects. This was already performed for gas mixture $\text{Ar}:\text{CO}_2:\text{N}_2$ 96:3:1, which did not show any indications for ageing [24]. This is expected for the other candidates as well. Furthermore, their performance under gamma and neutron radiation, in particular in view of a large neutron absorption cross section of a nitrogen isotope has to be studied. At gamma rates of 19 000 Hz/cm^2 the considerably less resolution deterioration at the use of the drift gas $\text{Ar}:\text{CO}_2:\text{N}_2$ 96:3:1 has already been experimentally proven in [16].

Bibliography

- [1] http://en.wikipedia.org/wiki/Large_Hadron_Collider.
- [2] http://fyzika.fs.cvut.cz/eng/Cooling/AtlasWeb/Atlas_1.htm.
- [3] <http://public.web.cern.ch/public/en/LHC/HowLHC-en.html>.
- [4] Rob Veenhof, <http://garfield.web.cern.ch/garfield/>.
- [5] Stephen Biagi, <http://magboltz.web.cern.ch/magboltz/>.
- [6] *ATLAS Muon Spectrometer - Technical Design Report*. Technical report, ATLAS Muon Collaboration, CERN, 1997.
- [7] M. Aleksa: *Performance of the ATLAS Muon Spectrometer*. Technische Universität Wien, Dissertation, 1999.
- [8] M. Aleksa, *Nuclear instruments and Methods in Physics Research* **A 478** (2002), 135.
- [9] R. Avramidou, *Nuclear Instruments & Methods in Physics Research* **A 586** (2006), 672.
- [10] A.B. Balantekin, editors. *Review of particle Physics, Particle Data Group*, Band 37. Journal of Physics G, Nuclear and Particle Physics, 2010.
- [11] B. Bittner, *Nuclear instruments and Methods in Physics Research* **A 617** (2010), 169.
- [12] M. Deile: *Optimization and Calibration of the Drift-Tube Chambers for the ATLAS Muon Spectrometer*. Ludwig-Maximilians-Universität München, Dissertation, 2000.
- [13] M. Deile, *Nuclear instruments and Methods in Physics Research* **A 518** (2004), 65.
- [14] A. Engl, *Nuclear Science Symposium Conference Record, 2008. NSS '08. IEEE* Seiten 2274 – 2277.
- [15] A. Engl, *Nuclear instruments and Methods in Physics Research* **A 623** (2010), 9193.
- [16] A. Engl: *Precise Muon Drift Tube Detectors For High Background Conditions*. Ludwig-Maximilians-Universität München, Dissertation, 2011.

-
- [17] C. Grupen: *Teilchenphysik*. Bibliographisches Institut & F.A. Brockmann AG, 1993.
- [18] L. Huber: *Analyse der Pulsform und Untergrundeigenschaften von Ar-CO₂-N₂ Driftgasen an MDT-Driftrohren*. Ludwig-Maximilians-Universität München, Bachelor thesis, 2009.
- [19] K. Kleinknecht: *Detektoren Für Teilchenstrahlung*. B. G. Teubner Stuttgart, 1984.
- [20] P. Lang: *Studien zur Gasmischung an MDT-Myon-Detektoren*. Ludwig-Maximilians-Universität München, Diploma thesis, 2008.
- [21] W. Leo: *Techniques for Nuclear and Particle Physics Experiments*. Springer-Verlag, 1987.
- [22] D.R. Lide, editors. *CRC Handbook of Chemistry and Physics*. CRC Press. Boca Raton, Florida, 2003.
- [23] M. Livan, *Nuclear instruments and Methods in Physics Research A* **384** (1996), 214.
- [24] A. Ruschke: *Erzeugung von hochenergetischen Neutronen und Protonenbestrahlungen an ATLAS Driftrohren*. Ludwig-Maximilians-Universität München, Diploma Thesis, 2010.
- [25] F. Sauli: *Principles of Operation of Multiwire Proportional and Drift Chambers, Lectures 1975 - 1976*. CERN - Service d'Information scientifique, 1990.
- [26] A. Souza, *J. Braz. Chem. Soc.* **5**, **No.2** (1994), 59.
- [27] G. Stark, *Journal of Quantitative Spectroscopy & Radiative Transfer* **103** (2007), 67.
- [28] A. Zibell: *Pulsformanalyse an MDT-Myondetektoren*. Ludwig-Maximilians-Universität München, Diploma Thesis, 2010.

Acknowledgment

I would like to thank...

- Prof. Dr. Otmar Biebel for giving me the opportunity to perform research in his group and being constantly helpful and supportive, especially for making my trip to CERN possible
- Dr. Ralf Hertenberger for the great assistance during the project, his willingness to answer all my questions and for being helpful with every problem
- Prof. Dr. Dorothee Schaile for the kind acceptance at her chair
- Jona Bortfeldt, Albert Engl, Alexander Ruschke and Andre Zibell for introducing me to the every day procedures, their help with the experiments and data evaluation, their supervision at CERN and for steadily being in a good mood
- all members of the Lehrstuhl Schaile for their friendliness and the fun during numerous table tennis games and else where
- my family for being understanding and supportive in every way
- Sebastian Gude

Erklärung:

Hiermit erkläre ich, die vorliegende Arbeit selbständig verfasst zu haben und keine anderen als die in der Arbeit angegebenen Quellen und Hilfsmittel benutzt zu haben.

München, 26. August 2011

Nicola Tyler